# Multiphysics Experimental Approaches for Insight into the Hydrogen Bonded Structures of Ethylene Glycol and Glycerol Mixtures toward Green Solvent Technology

Mukul Saraswat & R J Sengwa[*]

Dielectric Research Laboratory, Department of Physics, Jai Narain Vyas University, Jodhpur 342 005, India

Alcohols and their mixtures are credited most important polar solvents for advances in pharmaceutical, chemical, biological, thermal, and material technologies. A rigorous study for the characterization of hydrogen bonded heterogeneous intermolecular structures that formed in a mixed solvent based on alcohols containing two and three hydroxyl groups molecules is crucial to specific technological and industrial applications. Hence, in this work, the multiphysics experimental approaches including the measurements of dielectric, electrical, viscous, acoustic, thermal, and optical properties are applied and analyzed to confirm the behaviour of hydrogen bonded molecular structures of ethylene glycol (EG; dihydric alcohol) with glycerol (Gl; trihydric alcohol) over the entire concentration range of EG+Gl mixtures at 298.15 K. The static dielectric permittivity, direct current electrical conductivity, low frequency relaxation time, and refractive index values of the EG+Gl mixtures are reported. Additionally, dynamic viscosity, density, ultrasound velocity, adiabatic compressibility, intermolecular free length, acoustic impedance, free volume, Rao's constant, Wada constant, and viscoacoustic relaxation time of the EG+Gl mixtures are determined, and also explored their significance to these alcohols molecular interactions. Ultraviolet-visible range absorbance behaviour of the alcohol mixtures is characterized in detail and confirmed the electronic transitions at higher energy ultraviolet radiations. The detailed analysis of all the experimental results along with the consideration of excess properties evidenced the formation of heterogeneous intermolecular hydrogen bonded structures in these Newtonian-type alcohols mixtures. A small to adequate variation in the thermodynamical and other investigated properties with the concentration variation showed that the EG+Gl mixture can be optimized as a green solvent according to the prerequisite properties for huge advances in soft condensed matter technologies.

Keywords: Alcohols; Molecular interaction; Dielectric properties; Viscosity; Acoustic parameters; UV-Vis absorbance

## 1 Introduction

Understanding of molecular structures and dynamics in pure polar liquids (homogeneous systems), polymeric solutions in polar liquids (complex systems), and the binary and ternary mixtures of different polar liquids (heterogeneous systems) remained an immense academic interest, as well as an increasing industrials demand to optimize appropriate quality solvents and mixed solvents to meet the wide range of technological applications[1–12]. The hydrogen bonded polar liquids and their mixtures play an important role in all the areas of soft condensed matter physics, industrial chemistry, cosmetic and pharmaceutical industries, and biological and smart material related technologies[1–6,12–18]. So far, several attempts were made for the structural characterization of a variety of complex liquid solvents by determination of dielectric permittivity and relaxation processes[1–3,5–7,11–22], electrical conductivity[11–14,18,23], thermophysical properties[3,9,12,16,17], optical[4,24], and acoustic parameters[9,25]. Besides the uses as regular solvents for various applications, the associating green liquids EG and Gl, and these liquids mixtures based nanofluids were identified as promising heat transfer mediums in all kinds of heating and cooling processes, such as air conditioning, automobiles, refrigeration systems, solar energy harvesting and storage systems, nuclear and thermal power plants, space and defence systems, and also in microelectronic devices[26–34].

Among the hydrogen-bonded liquids, alcohols (mono-, di-, and tri-hydric) and their mixtures with other polar liquids are established as the most suitable solvents for a wide range of technological applications[1–5,8–12,16,17,33–38]. The dihydric alcohol, that is EG, is one of the important polar organic

―――――――――
*Corresponding author: (E-mails: rjsengwa@rediffmail.com;
rjs.ph@jnvu.edu.in)

compounds and chemical intermediate due to its unique thermophysical properties such as colourless, odourless, viscous, lubricant, hygroscopic, and also relatively low-volatile, low toxicity, high dielectric constant, and a stronger ability to form complexes with additives through hydrogen bonding[1,5,26–29,31,33,35,37,38]. In the chemical formula of the EG molecule (HO–CH$_2$–CH$_2$–OH), there are two hydroxyls groups (–OH) on adjacent carbon atoms which have a strong tendency to form intra- and intermolecular hydrogen bonded structures in the pure liquid state[33,37,38], because of this fact its viscosity and boiling temperature are relatively high. The liquid EG is completely miscible with many other polar solvents including water, most of the aliphatic alcohols, amides, amines, etc., owing to the formation of heterogeneous hydrogen bonding through the ends hydroxyl groups of its EG molecules[1,3,5,8,33,35].

In the family of alcohols, the Gl is recognized as a green polar solvent with versatile industrial and technological uses[34,36,39]. Similar to other alcohols, the Gl is colourless, odourless, low-cost, highly miscible, and additionally less hazardous having ultrahigh viscosity, as well as high boiling point and the dielectric constant[34-36,39–42]. Furthermore, Gl is primarily derived from the natural and petrochemical feedstock[39], and therefore it is one of the economical green chemistry solvent materials. In the chemical formula of the Gl molecule, that is (OH–CH$_2$–CH(OH)–CH$_2$–OH), all the three active alcoholic hydroxyl groups are responsible for the high solubility and hygroscopic nature, and are also recognized as a potential candidate for catalysis applications[34]. The structural arrangement of the three –OH groups (two as primaries and one as secondary) in the molecular structure of the Gl categorized it as propane-1,2,3-triol in IUPAC nomenclature. The Gl molecules are highly interactive, forming both intra- and intermolecular hydrogen bonds in the pure liquid state[7,34,35,38,41], and also the heterogeneous hydrogen bonds in the mixtures with a variety of polar liquids[3,7,8,35,40,42]. In regards to the practical applications of the liquids for fluid flow and heat transfer, besides the need for high boiling temperature and thermal stability, viscosity is a very important property because convective heat transfer and pumping power in the flow systems are proportionally linked to the viscosity of the fluid[36,43,44]. The ultrahigh viscosity of the liquid Gl, over a broader temperature range, established it as the most appropriate heat transfer fluid for energy transportation in the flow systems[10,30,36,43–45].

Dielectric studies on the EG and Gl systems confirmed that the molecular dipole moment μ of the EG molecule (μ = 2.38 D) is slightly lower than that of the Gl molecule (μ = 2.56 D) which is because of the difference in the number of –OH dipoles and their positional arrangement, whereas both these liquids have nearly equal values of the static dielectric permittivity $\varepsilon_s$ at a fixed temperature of 298.15 K (EG $\varepsilon_s$ = 41.12 and Gl $\varepsilon_s$ = 42.49) confirming their same magnitude of molecular dielectric polarization[37,38]. The Kirkwood correction factor $g$ is a measure of hydrogen bonded parallel or antiparallel aligned dipole ordering in a polar liquid. The $g$ values for the EG and Gl liquids are 2.35 and 2.70, respectively[37,38] which ascribed the stronger intermolecular hydrogen bonding with parallel dipole alignments in these liquid systems. From the relative $g$ values of these alcohols, it was also explained that the Gl molecules exhibited cross-linked hydrogen bonded structures owing to the presence of three hydroxyl groups in its molecules which caused relatively high viscosity[30,34,36,38,41]. The microwave frequency range dielectric dispersion study on the EG and Gl systems provided a relatively longer molecular reorientation relaxation time $\tau_0$ for the Gl molecules ($\tau_0$ = 1247 ps) which is about thirteen times higher than the EG molecules ($\tau_0$ = 92.4 ps) at 298.15 K[38]. Considering the various dielectric parameters of these di- and tri-hydric molecules, it was demonstrated that a longer one dimensional (1D) chains like structures are formed by the associated EG molecules and then the cross-linkage of the chains through H-bonded turned into two dimensional (2D) network[2,37,38], whereas stronger hydrogen bonded three-dimensional (3D) semicrystalline network is formed by the Gl molecules in the pure liquid state[2,15,22,30,38].

According to the literature survey, the dielectric and electrical characterizations of a variety of polar liquids and mixtures are needed to understand their polarization strength and insulation behaviour for exploring a wide range of industrial applications, and such study also has great interest from an academic standpoint to design appropriate theoretical models describing the experimental data[1,2,5–8,16–22,40,42,46–49]. In the last decades, immense work on dielectric properties was carried out to reveal the structural complexity and dynamics of the hydrogen bonded heterogeneous molecular networks in the liquid mixtures containing EG and Gl as one of the constituents[1,5,7,35,42]. In addition to the study of

dielectric properties, the structures of liquid mixtures are frequently examined by the determination of excess thermophysical properties like excess volume, density, viscosity, enthalpy of mixing, ultrasound velocity, compressibility, *etc*.[4,6,9,16,17,25,50–56]. Many of the results demonstrated that the deviation of properties from the thermodynamically ideal liquid mixtures, and also the detailed analysis of excess dielectric constant as well as other aforesaid thermophysical parameters altogether firmly justify the nature of hydrogen bonding and strength of heterogeneous intermolecular interactions in the mixtures of polar liquids. It is expected regarding the ideal liquid binary mixture that the values of various thermodynamical parameters should be a linear function of the composition constituent concentration. However, regarding an ideal liquid mixture, the choice of component scale (either volume fraction or mole fraction) remains an unsolved but widely used option is the one that leads to volume-fraction additivity of ideal relative permittivity[16,17,20,21,48]. Earlier, the volume fraction-weighted additively law was demonstrated in detail for describing the dielectric permittivity of liquid mixtures and confirmation of heterogeneous molecular interactions[21]. For the analysis of H-bond interactions between EG and Gl molecules, we applied the volume fraction and also the mole fraction additivity law in the EG+Gl mixtures in this manuscript.

To the best of our review, there is a lack of experimental data on the complex dielectric permittivity, electrical conductivity, viscous, acoustic, and optical properties of the EG+Gl mixtures to date. Systematic characterization of these different properties of two and three hydroxyl groups containing alcohol molecules-based liquid binary mixtures is needed especially for their practical applications as conventional heat transfer fluid and also the use as base fluid in the preparation of promising properties nanofluids. In the present paper, we have studied the 20 Hz to 1 MHz range harmonic electric field frequency-dependent complex dielectric permittivity ($\varepsilon'$ and $\varepsilon''$), and then deduced the complex electric modulus ($M'$ and $M''$), electrical impedance ($Z'$ and $Z''$) and the alternating current (ac) electrical conductivity ($\sigma'$ and $\sigma''$) as well as the low frequency dielectric relaxation processes of the EG+Gl mixtures, at a fixed temperature of 298.15 K. In these complex dielectric and electrical quantities, the notations single prime and double prime denote the real part and the

imaginary part, respectively. Additionally, the values of static and high-frequency limiting dielectric permittivity, excess dielectric permittivity, and the direct current (dc) electric conductivity of the EG+Gl mixtures are determined and discussed to understand the nature of heterogeneous hydrogen bonded structures in these mixtures. The detailed dielectric and electrical characterization of the EG+Gl systems will also help in confirming their uses as liquid electrical insulators, and also in the design of appropriate polarization strength solvents for a wide range of technological applications.

In this work, a study on thermophysical properties such as viscosity, density, free volume, ultrasound velocity, and thermal conductivity is also performed to explore in-depth the behaviour of H-bonded heterogeneous molecular interactions in the EG+Gl mixtures, and to support the results concluded on their structural behaviour from the dielectric properties. Furthermore, the viscosity and thermal conductivity data have a special interest in regards to the design of appropriate fluid or nanofluid for the heat transfer purpose in different kinds of thermal systems. More detail about the nature of H-bonded structures in the EG+Gl mixtures is explained by the determination of intermolecular free space length, adiabatic compressibility, acoustic impedance, viscoacoustic relaxation time, Rao's constant, Wada constant, and also the excess properties of some of these acoustic parameters. Furthermore, an attempt is made to characterize the ultraviolet-visible (UV-Vis) range absorbance behaviour for confirmation of hydrogen bond heterogeneous molecular interaction formed, and their effect on electronic transitions in the EG+Gl mixed systems. These UV-Vis experimental data can identify the possible use of EG+Gl mixtures in the design of soft condensed matter related optical materials. Herein, we have used multiphysics measuring methods for the determination of different properties of the EG+Gl mixtures which all provide complementary information on the H-bonded structures of the mixtures and changes therein with concentration variation.

## 2 Experimental

### 2.1 Materials

Glycerol (Gl; molar mass $M_w$ = 92.09 g·mol$^{-1}$) for spectroscopy grade with purity > 0.99, was purchased from HiMedia Laboratories Pvt. Ltd., India. The analytical reagent (AR) grade ethylene glycol (EG; molar mass $M_w$ = 62.07 g·mol$^{-1}$) of purity > 0.995 was

obtained from Loba Chemie Pvt. Ltd., India. The different volume concentration binary mixtures of the EG and Gl (herein these binary mixtures are labelled as EG+Gl) were prepared into stoppered glass bottles to prevent evaporation and environmental contamination. Initially, the required volumes of the EG and the Gl were mixed, at 298.15 K, by syringing with a precision volume syringe into the bottles. Then the correct values of corresponding volumes were verified by simultaneously measuring the masses of the liquids with the density values of pure liquids. A Wenser MAB-250 analytical electronic balance with a standard uncertainty of 0.01 mg was used for the mass measurements. All the EG+Gl mixtures were prepared in a single laboratory session with maintaining uniform preparation conditions. Homogeneity of the mixtures was performed by magnetic bar stirring at room temperature. From the values of volumes for the constituents in the EG+Gl mixtures, the volume fractions of the EG (denoted by $\phi_{EG}$) and Gl (denoted by $\phi_{Gl}$, which is equal to $1-\phi_{EG}$) were obtained. The standard uncertainty of the volume fraction values of the constituents ($\phi_{EG}$ and $\phi_{Gl}$) in the prepared EG+Gl mixtures is found to be 0.001. Further, the mole fraction values of the constituents of these EG+Gl binary liquids were determined from the measured values of their masses in the mixtures.

### 2.2 Apparatus and Measurements

Agilent Technologies Pvt. Ltd. made a precision inductance-capacitance-resistance (LCR) meter having a 1-volt amplitude oscillator of frequency range from 20 Hz to 1 MHz (model: 4284A), and its compatible parallel plates four-terminals liquid test fixture (model: 16452A), were used for the measurements of capacitance ($C_p$) and resistance ($R_p$) of the liquid samples. From these $C_p$ and $R_p$ values the frequency-dependent values of complex dielectric permittivity $\varepsilon^*(\omega) = \varepsilon' - j\varepsilon''$ of the EG+Gl mixtures were determined at 298.15 K using the expression given in section 3.1.1. The static dielectric permittivity $\varepsilon_s$ determined from the measurements of experimental high frequency (1 MHz) $\varepsilon'$ value has a relative standard uncertainty of 1%.

The high-frequency limit optical dielectric constant $\varepsilon_\infty$ of the samples was taken as the square of the refractive index $n_D$, which was measured at 298.15 K, by employing the thermostated Abbe refractometer operated at a wavelength of sodium D-light. The refractometer was calibrated with deionized water and the standard uncertainty of the measurements is 0.0001.

The dynamic viscosities $\eta$ of these liquid samples were measured using a Fungilab Alpha L-series rotational viscometer having fully microprocessor controlled operation with a digital display. It was equipped with an APM sample adapter cell of 8 mL capacity along with a cylindrical spindle TL-5 and the provision of a water circulation jacket for the thermostat. Before taking sample measurements, this instrument was calibrated following the manufacturer's operating instruction manual. The viscosity was recorded by rotating the spindle over the shear rate range from 0.396 s$^{-1}$ to 80 s$^{-1}$ (depending on the sample viscosity) with maintaining the required torque in the range provided by the manufacturer (*i.e.*, 15% to 100%) for the relative standard uncertainty of 1%. These rheological measurements were made at the fixed temperature of the sample filled in a thermostated cell, at 298.15 K.

The densities $\rho$ of these liquid samples were measured with a precision relative density bottle of 10 mL volume caped with a fine capillary Teflon cap (Borosil Glass Works Ltd. Catalogue Code 1624006). For the measurements, initially, the mass of the empty bottle was noted using an analytical electronic balance (Wensar MAB-250). Thereafter, the bottle was filled with a sample covering the full length of the capillary, at 298.15 K, and its mass was remeasured. From these measurements, the mass of the filled sample in the bottle was obtained. The density of the sample was determined by taking the ratio of the mass to the volume with a measurement standard uncertainty of 0.005 kg/m$^3$.

The ultrasound velocity $u$ of the samples was measured with a nanofluid interferometer (Mittal Enterprises, model: NF-10X) which was operated at the ultrasound wave of frequency 2 MHz. This interferometer apparatus was equipped with a thermostated test cell TC–2 fitted with a digital micrometer of resolution 0.001 mm to record the movable plunger position. The interferometer was calibrated with double distilled water and the standard uncertainty in the measured velocity of ultrasound was 0.2 m·s$^{-1}$. For this, the sample was filled in the test cell and the ultrasound velocity of the propagating wave was determined by noting the wavelength of the standing wave formed in the sample by a shorted movable plunger. The wavelength of the standing wave

was correctly measured by taking the digital micrometer readings at the positions of several successive minima and also the maxima with driving the plunger.

In all these experiments the temperature of the sample under measurements was regulated with a repeatability of 0.02 K. For this purpose a Thermo-Haake DC 10 controller was used that fitted to the water circulating bath of Escy Enterprises Pune, India, having simultaneous heating and cooling control devices.

The ultraviolet-visible (UV-Vis) range absorbance by the EG+Gl liquid samples for the incident photons of the wavelength range from 200 nm to 1100 nm, was recorded at ambient temperature using a dual-beam UV-Vis spectrophotometer with a wavelength resolution of 1 nm (Agilent Technologies Pvt. Ltd., model - Cary 60). It is a computer-controlled instrument operated with the Cary WinUV software. Before sample measurements, the baseline correction with an empty quartz cuvette was performed at a scan rate of 10 nm/s. Thereafter, the sample was filled in the cuvette of 3 mL volume and 1 cm width for light travel, and then the absorbance was recorded with baseline correction.

## 3 Results and discussion

### 3.1 Dielectric and Electrical Properties

#### 3.1.1 Dielectric Permittivity Spectra

The complex dielectric permittivity $\varepsilon^*(\omega)$, as a function of angular frequency $\omega$, is determined from the relationship given in Eq. (1);

$$\varepsilon^*(\omega) = \varepsilon' - j\varepsilon'' = \alpha\left(\frac{C_P}{C_0} - j\frac{1}{\omega C_0 R_P}\right) \qquad \dots (1)$$

In Eq. (1) the real part $\varepsilon'$ of the complex permittivity is a measure of the electrical energy storage ability of the dielectric material, and the imaginary part $\varepsilon''$ represents an average energy loss per cycle due to the joules heating effect. The notation $\omega$ is given by $\omega = 2\pi f$, where $f$ is the applied harmonic electric field linear frequency. $C_0$ and $C_p$ are the experimental values of the capacitances of the empty dielectric fixture (without sample) and filled with the sample, respectively, and $R_p$ is the equivalent parallel resistance of the sample filled test fixture. The $\alpha$ is a correction coefficient of the liquid dielectric test fixture which is introduced for the cancellation of stray capacitance and leads resistance to maintain the standards of dielectric and electrical measurements as set by the American Society for Testing and Materials

(ASTM), and the $\alpha$ values over the entire frequency range were provided by the manufacture.

Characterization of $\varepsilon'$ and $\varepsilon''$ as a function of frequency covering a wide range is needed for exploring vital technological applications of the dielectric material. The values of $\varepsilon'$ and $\varepsilon''$ as a function of frequency $f$ over the 20 Hz to 1 MHz range for the EG+Gl mixtures, at a fixed temperature of 298.15 K, are plotted in Fig. 1. According to the appeared dispersion behaviour of $\varepsilon'$ values with frequencies for the different volume concentrations of Gl ($\phi_{Gl}$) in the EG+Gl mixtures, these plots can be divided into two parts with respect to the frequency scale. The first part covers the low-frequency range from 20 Hz to about 200 Hz where the $\varepsilon'$ values decrease sharply with the increase of frequency. This part for the EG+Gl systems can be assigned to the dominant contribution of the electrode polarization (EP) process which is demonstrated previously for
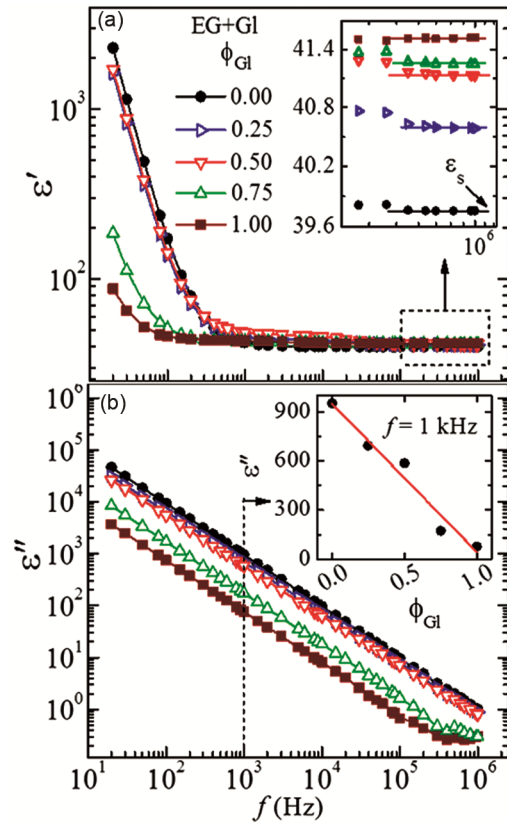


Fig. 1 — Plots of complex dielectric permittivity real part $\varepsilon'$ and imaginary part $\varepsilon''$ versus frequency $f$ for the EG+Gl mixtures with different volume fraction concentrations of Gl ($\phi_{Gl}$ = 0.00, 0.25, 0.50, 0.75, and 1.00), at 298.15 K. Inset of (a) shows the enlarged view of $\varepsilon'$ values in the 100 kHz to 1 MHz range corresponding to the static permittivity region and the inset of (b) shows the $\varepsilon''$ versus $\phi_{Gl}$ plot at $f$ = 1 kHz.

several polar liquids[11–14,18]. This dispersion behaviour of the ε′ values for the dielectric materials such as polar liquids and their mixtures deal with the formation of electric double layers (EDLs) capacitances at the test fixture electrodes and dielectric interfaces. The EDLs are formed by the accumulation of long distance drifted charges which are activated in a polar liquid dielectric sample due to various sources given in the literature[13,18,23,57]. The accumulation of charges at the electrode-dielectric interfaces occurs when there is a slow reversal of the applied low frequency harmonic electric field which is explained in detail previously for several polar liquid materials[11–14,18,57–61]. Furthermore, the higher ε′ values appeared in the lower frequency part of these spectra, for the pure EG and the EG-rich sample of the EG+Gl mixtures in comparison to that of the pure Gl and the Gl-rich sample, revealing a stronger contribution of the EP-process in the EG liquid.

The second part of the ε′ spectra of these liquid dielectrics, having an onset frequency of about 200 Hz and extending up to 1 MHz, exhibited a little change in the ε′ values with the frequency variation, and lastly turned to be frequency independent that represents the static dielectric permittivity ε_s of these materials. The measure of ε_s denoted the magnitude of molecular polarization of the polar dielectric liquid systems, and therefore the ε_s measurement of most of the liquid dielectrics with high accuracy is performed by applying the harmonic electric field of frequency around 1 MHz[6,11,12,16,20,21,35,62,63]. The inset of Fig. 1(a) explains that at about the end frequencies of these spectra, the ε′ value of pure Gl is slightly higher than that of the pure EG confirming a relatively more strength of molecular polarization of the Gl system. The ε_s values which are taken equal to the ε′ values at 1 MHz (marked by horizontal solid lines in the inset of Fig. 1(a) for these EG, Gl, and EG+Gl systems at a fixed temperature of 298.15 K are given in Table 1, from which a comparative variation in ε_s values for

these mixtures can be noted. The ε_s values of the pure EG and pure Gl, listed in Table 1, are also found in good agreement with their literature data[7,35,37,38].

On the log-log scale, the ε″ values for all these EG+Gl systems exhibited a linear decrease as the frequency of electric field augments in the experimental frequency range (Fig. 1(b)). The slopes of ε″ versus f plots for these dielectric materials are found close to unity confirming that the dielectric losses are predominantly due to the Ohmic type ionic conduction which is a common cause for the origin of low frequency dielectric losses in the polar liquids[11–14,18,57,59,60,64]. Further, the frequency dependent ε″ values of the Gl liquid are lower than that of the EG liquid revealing that the ions transport is also influenced by the H-bonded structural driven mechanism in these liquid systems. A plot of ε″ versus $\phi_{Gl}$ (at f = 1 kHz) on the linear scale is shown in the inset of Fig. 1(b) revealing that there is an almost linear decrease in ε″ values, at a fixed frequency, when the Gl volume fraction increases in the EG+Gl mixtures. This finding is interesting in regards to controlling the amount of ion conduction by simply adjusting the constituent concentration of the EG+Gl mixture.

The dielectric loss tangent angle, denoted by tanδ (ε″/ε′) which is equal to the inverse of quality factor Q, is one of the important dielectric parameters. The dielectric materials of low tanδ values with the high ε′ confirm their suitability in the fabrication of high-performance energy storing capacitive devices. The tanδ versus f plots for the binary mixtures of EG+Gl, at 298.15 K, are presented in Fig. 2. It is a useful presentation for the analysis of the EP-relaxation process which is thoroughly explained for a wide range of polar liquid materials in the literature[13,14,18,57–60]. Important characteristics of these tanδ versus f plots are, firstly an intense relaxation peak has appeared for the pure EG and EG+Gl binary mixtures in the lower experimental frequency range and

Table 1 — The values of static dielectric permittivity ε_s, refractive index $n_D$, high-frequency limit dielectric constant $\varepsilon_\infty$, the dielectric strength Δε, electrode polarization relaxation time $\tau_{EP}$, charge conductivity relaxation time $\tau_\sigma$, dc electrical conductivity $\sigma_{dc}$, viscosity η, and the product $\sigma_{dc}\cdot\tau_\sigma$, and $\sigma_{dc}\cdot\eta$ for the binary mixtures of EG+Gl with varying Gl volume fraction concentration $\phi_{Gl}$, at 298.15 K.

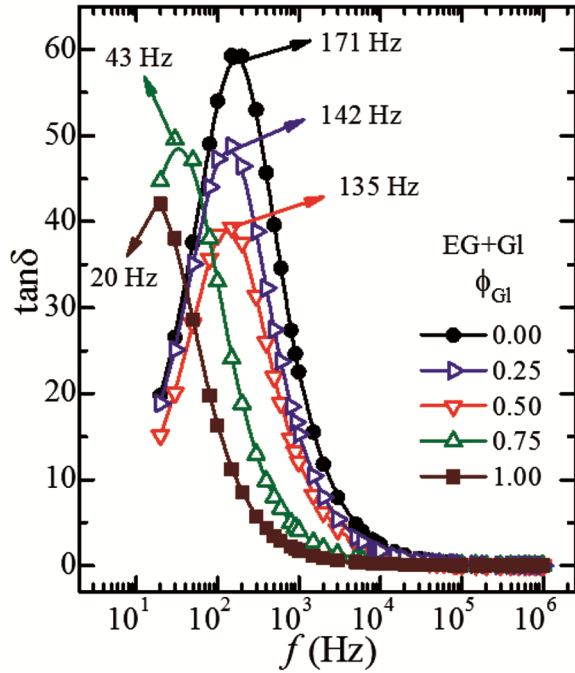| $\phi_{Gl}$ | $\varepsilon_s$ | $n_D$ | $\varepsilon_\infty$ | Δε | $\tau_{EP}$ (ms) | $\tau_\sigma$ (μs) | $\sigma_{dc}\times10^7$ (S·cm$^{-1}$) | η (mPa·s) | $\sigma_{dc}\cdot\tau_\sigma\times10^{12}$ (S·cm$^{-1}$·s) | $\sigma_{dc}\cdot\eta\times10^3$ (S·m$^{-1}$·Pa·s) |
|---|---|---|---|---|---|---|---|---|---|---|
| 0.00 | 39.75 | 1.4239 | 2.027 | 37.72 | 0.93 | 6.40 | 5.23 | 15 | 3.3 | 0.78 |
| 0.25 | 40.59 | 1.4361 | 2.062 | 38.53 | 1.12 | 8.96 | 3.55 | 30.3 | 3.2 | 1.08 |
| 0.50 | 41.19 | 1.4430 | 2.082 | 39.05 | 1.18 | 10.90 | 2.96 | 61.4 | 3.2 | 1.82 |
| 0.75 | 41.25 | 1.4550 | 2.117 | 39.13 | 3.70 | 34.30 | 0.97 | 154.1 | 3.3 | 1.49 |
| 1.00 | 41.52 | 1.4671 | 2.152 | 39.37 | 7.96 | 88.44 | 0.42 | 733.2 | 3.7 | 3.08 |

Fig. 2 — Plots of dielectric loss angle tangent tanδ versus frequency $f$ for the EG+Gl mixtures with different volume fraction concentrations of Gl ($\phi_{Gl}$ = 0.00, 0.25, 0.50, 0.75, and 1.00), at 298.15 K. The frequency values corresponding to the electrode polarization relaxation process are labelled on the respective plot.



Fig. 3 — Plots of relaxation times $\tau_{EP}$ and $\tau_\sigma$ versus volume fraction concentration of Gl $\phi_{Gl}$ for the EG+Gl mixtures, at 298.15 K. The experimental data are joined with B-spline. The dashed straight line represents the linear dependency on volume fraction-weighted additivity law and the solid line is the polynomial fit of experimental data.

showed a shift towards the low frequencies when the concentration of Gl in the mixtures was enhanced. The trend of shifts in this relaxation peak on the frequency scale with the increase of $\phi_{Gl}$, reflects that the pure Gl has a relaxation peak around 20 Hz at 298.15 K, and therefore this lowest experimental frequency value is taken as its relaxation frequency. Secondly, it is noted from this figure that the relaxation peak for the neat EG is relatively more intense and its position on the frequency scale is located corresponding to the frequency at which onset steep increase of the ε′ values appeared (see Fig. 1(a) for frequency matching) and therefore this peak can be assigned to the electrode polarization relaxation process. Additionally, it was noted that the tanδ peak intensity value first decreases with the increase of $\phi_{Gl}$ values up to 0.5, and thereafter, it increases again for the Gl-rich mixture of EG+Gl system which suggests some correlation of ion transportation with the viscosity of the mixture.

The mechanism of EDLs charging and discharging can be explored by the determination of EP-process relaxation time $\tau_{EP}$ for these binary mixtures of EG+Gl with the tanδ peak frequency $f_p$ dependent relationship as given in Eq. (2) [11,12,57,64];
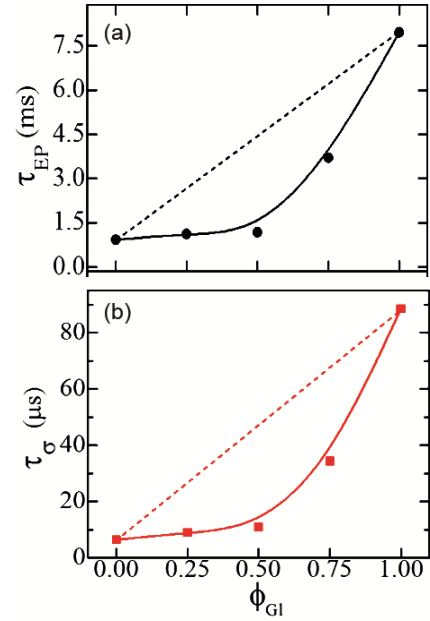
$$\tau_{EP} = 1/2\pi f_p \qquad \qquad \dots (2)$$

The obtained $\tau_{EP}$ values for the EG+Gl mixtures are listed in Table 1, and these are also potted against $\phi_{Gl}$ in Fig. 3(a). This figure explains that there is an insignificant increase in $\tau_{EP}$ values in the EG-rich mixtures with an increase of $\phi_{Gl}$ concentration up to 0.5, but it showed a relatively huge increase for the Gl-rich concentration range of EG+Gl mixtures. This finding characterizes the charging and discharging process of the EDL capacitances ruled by the dominant concentration constituents in these EG+Gl liquid mixtures. Furthermore, the observed low $\tau_{EP}$ values as compared to the linear dependency (marked by a dashed straight line in Fig. 3(a)) reveal that the EDL process occurs relatively faster in the EG+Gl mixtures.

Static dielectric permittivity $\varepsilon_s$ values of the EG+Gl mixtures as a function of $\phi_{Gl}$ are presented in Fig. 4. Although, the $\varepsilon_s$ values of pure EG and pure Gl liquids are nearly equal ($\varepsilon_{s(Gl)}$ = 41.52 which is slightly higher than that of $\varepsilon_{s(EG)}$ = 39.75 at 298.15 K) beside this fact the plot of $\varepsilon_s$ versus $\phi_{Gl}$ confirms that there is a non-linear increase in $\varepsilon_s$ values with the increase of $\phi_{Gl}$ in these binary mixtures. A significant deviation in
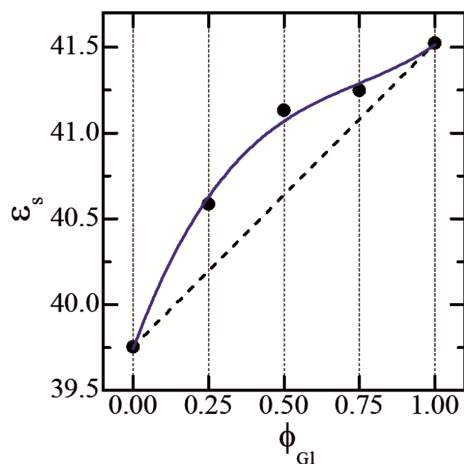
Fig. 4 — The plot of static dielectric permittivity $\varepsilon_s$ against volume fraction concentration of Gl $\phi_{Gl}$ for the EG+Gl mixtures, at 298.15 K. The dashed straight line represents the linear dependency on volume fraction-weighted additivity law and the solid line is the polynomial fit of experimental data.

the experimental $\varepsilon_s$ data from the thermodynamically ideal liquid mixtures behaviour[21] (marked by the dashed lines in Fig. 4) confirms that the EG+Gl systems are non-ideal from a dielectric mixing point of view. This finding evidences that there is some alteration of the parallel dipolar ordering in the homogeneous molecular structures of the neat EG and neat Gl which supports the heterogeneous hydrogen bond formation in the studied mixtures. Furthermore, the obtained positive deviation in $\varepsilon_s$ values for the EG+Gl mixtures as compared to the ideal liquid mixture behaviour reveals some increase in the number of parallel dipole ordering of the molecules which causes by the formation of some heterogeneous molecular aggregate besides the existence of 1D chain structures of EG molecules and 3D supramolecular structure of Gl molecules in the EG+Gl mixtures.

### 3.1.2 Electric Modulus Spectra

The real part $M'$ and imaginary part $M''$ of the complex electric modulus $M^*(\omega)$ for the EG+Gl mixtures at different frequencies of the harmonic electric field in the experimental frequency range were computed by substituting the corresponding frequencies $\varepsilon'$ and $\varepsilon''$ values in the relationship given as Eq. (3)[14,18,57,64];

$$M^*(\omega) = \frac{1}{\varepsilon^*(\omega)} = M' + jM'' = \frac{\varepsilon'}{(\varepsilon')^2 + (\varepsilon'')^2} + j\frac{\varepsilon''}{(\varepsilon')^2 + (\varepsilon'')^2} \quad \dots (3)$$

The plots of $M'$ and $M''$ versus $f$ for the EG+Gl binary mixtures, at 298.15 K, are presented in Fig. 5. As can be seen from this figure that the $M'$ spectra of
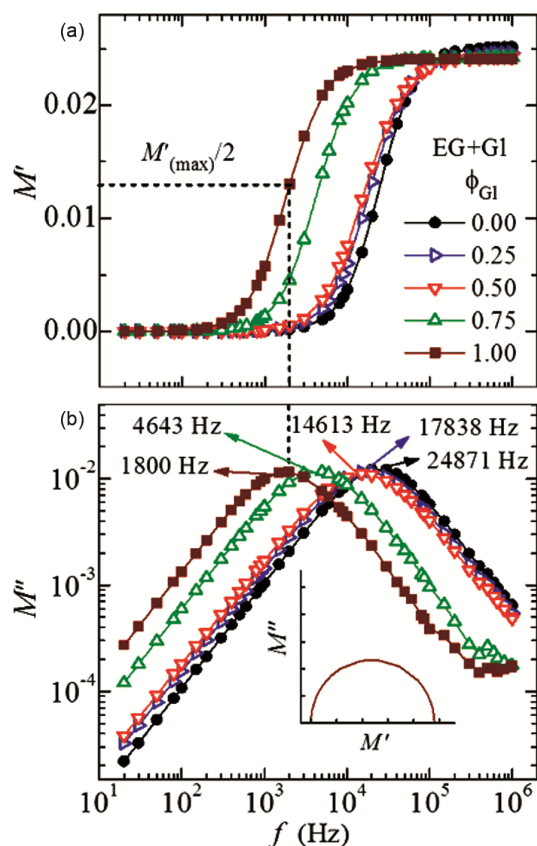


Fig. 5 — Complex electric modulus real part $M'$ and imaginary part $M''$ versus frequency $f$ plots for the EG+Gl mixtures with different volume fraction concentrations of Gl ($\phi_{Gl}$ = 0.00, 0.25, 0.50, 0.75, and 1.00), at 298.15 K. The frequency values corresponding to the ionic conduction relaxation process are labelled in (b). The vertical dashed line from (b) to (a) shows the peak position frequency at half of maximum $M'$ value marked as a horizontal dashed line with $M'_{(max)}/2$ (a). The Debye dispersion behaviour of $M''$ versus $M'$ complex plane plot is shown in the inset of (b) for the pure Gl as a representative plot.

the EG+Gl mixtures exhibited a step-like shape having about zero and maximum $M'$ values in the start and end frequencies regions, respectively, whereas a non-linear and large increase has appeared in the middle-frequency range. The $M''$ values have continuous variation with frequency and exhibited relaxation peaks in the middle frequency range corresponding to the ionic conduction relaxation process. The shape of these $M'$ and $M''$ spectra of the EG+Gl systems are found in agreement with several other pure polar liquids and their mixtures, except some shifts in the non-linear region of $M'$ and also the relaxation peak of $M''$ on the frequency scale[11-14,18,57,58,64]. Furthermore, as compared to the sharpness and change in intensities of the relaxation peaks that appeared in the tanδ spectra of the EG+Gl

mixtures, the $M''$ spectra of these mixtures exhibited broader relaxation peaks of almost the same intensities. Additionally, the position of these $M''$ relaxation peaks are noted relatively at the higher frequencies with a shift of one to two orders of magnitude as compared to the frequency positions of the tanδ peaks. A representative complex plane plot ($M''$ versus $M'$) for a neat Gl system, as shown in the inset of Fig. 5(b), confirms that the electric modulus spectra of these materials have Debye-type dispersion of the conductivity relaxation process. Therefore, with this fact of the symmetrical dispersion, taking the frequency values corresponding to the peaks from $M''$ spectra (herein denoted by $f_\sigma$ and values are marked on the respective spectra in Fig. 5) the conductivity relaxation time $\tau_\sigma$ of the EG+Gl materials are determined from the relationship given in Eq. (4)[14,18];

$$\tau_\sigma = 1/2\pi f_\sigma \qquad \qquad \dots (4)$$

The observed $\tau_\sigma$ values of these EG+Gl mixtures are listed in Table 1, and these values are also plotted as a function of $\phi_{Gl}$ in Fig. 3(b), for their comparative analysis with the respective $\tau_{EP}$ values. It can be noted from Fig. 3(b) that the variation of $\tau_\sigma$ with $\phi_{Gl}$ for these EG+Gl mixtures obey the similar trend as that of their $\tau_{EP}$ values. The observed lower $\tau_\sigma$ values as compared to the linear dependency of the mixture constituent concentration infer that the heterogeneous structures formed by the EG and Gl molecules promote the charge dynamics in the EG+Gl mixtures. The low value of $\tau_\sigma$ for the pure EG as compared to the pure Gl infers a relatively faster ions transport mechanism in the EG liquid 1D chain structure. Further, the $\tau_{EP}$ values of these EG+Gl systems are found more than two orders of magnitude higher as compared to their $\tau_\sigma$ values at a fixed temperature of 298.15 K (see Table 1). This finding also reveals that for a particular polar liquid system, there is a slower dynamic of the EP-process and a relatively faster occurrence of the conductivity relaxation process which is a characteristic behaviour previously revealed for several polar liquids and also complex liquid systems in the lower frequency regime[13,18,57–60,64,65]. Furthermore, in the higher broadband frequency range, there is a larger possibility of different origins of the molecular and dipolar relaxation processes in these H-bond associated EG+Gl mixtures. It is suggested that this point should be investigated with temperature variations in future work.

### 3.1.3 Electrical Conductivity Spectra

The alternating current (ac) electrical conductivity (real part σ′ and imaginary part σ″) values as a function of the $f$ over the frequency range of 20 Hz to 1 MHz, for the EG+Gl binary mixtures are determined from the proportionality relationship of complex conductivity with the complex permittivity as given in Eq. (5)[18,57,64];

$$\sigma^*(\omega) = \sigma' + j\sigma'' = j\omega\,\varepsilon_0\,\varepsilon^*(\omega) = \omega\,\varepsilon_0\,\varepsilon'' + j\omega\,\varepsilon_0\,\varepsilon'$$
$$\dots (5)$$

In the above relationship, $\varepsilon_0$ is the dielectric constant value for vacuum ($8.854 \times 10^{-12}$ F/m). The variation of σ′ and σ″ with $f$ for the EG+Gl binary mixtures at 298.15 K is demonstrated in Fig. 6. It can be noted from Fig. 6(a) that the σ′ values are independent of frequency in the lower experimental frequency range and this steady-state frequency span depends on the constituents composition of the EG+Gl mixtures. With consideration of this fact, the lower frequencies σ′ values were assigned to the direct current (dc) electrical conductivity $\sigma_{dc}$ of these polar liquid materials. The $\sigma_{dc}$ values noted from the low frequencies steady-state behaviour of the σ′ spectra (as marked by solid horizontal lines) for the EG+Gl systems are recorded in Table 1. The $\sigma_{dc}$ values of the formulated EG+Gl mixtures are found of the order of $10^{-7}$ S/cm and these show a decrease when the $\phi_{Gl}$ concentration in the mixtures increases. A gradual increase of σ′ at higher frequencies reflects the turning of dc to ac transport of the charge carriers as mostly noted and explained for a variety of polar liquids and soft materials[11,13,18,30,57,58,64]. The σ″ spectra of these EG+Gl liquid materials at 298.15 K (Fig. 6(b)) appear overlapped over the wider frequency range from ∼ 200 Hz to 1 MHz, and also showed a linear increase when the frequency was increased, confirming the dominance effect of dc ionic conduction in this experimental frequency range[60]. A deviation in the σ″($f$) values from linearity in the starting narrow window of experimental frequencies (20 Hz to about 200 Hz) confirms a dominance contribution of the EP effect in the ac electrical conduction behaviour of these EG+Gl mixtures.

Figure 6(c) illustrates that there is an inverse relationship between the $\sigma_{dc}$ and $\tau_\sigma$ values of the EG+Gl mixtures, which means the increase of $\tau_\sigma$ values reduce the $\sigma_{dc}$ values that are attributed to slow down in mobility of the transporting charge carriers as
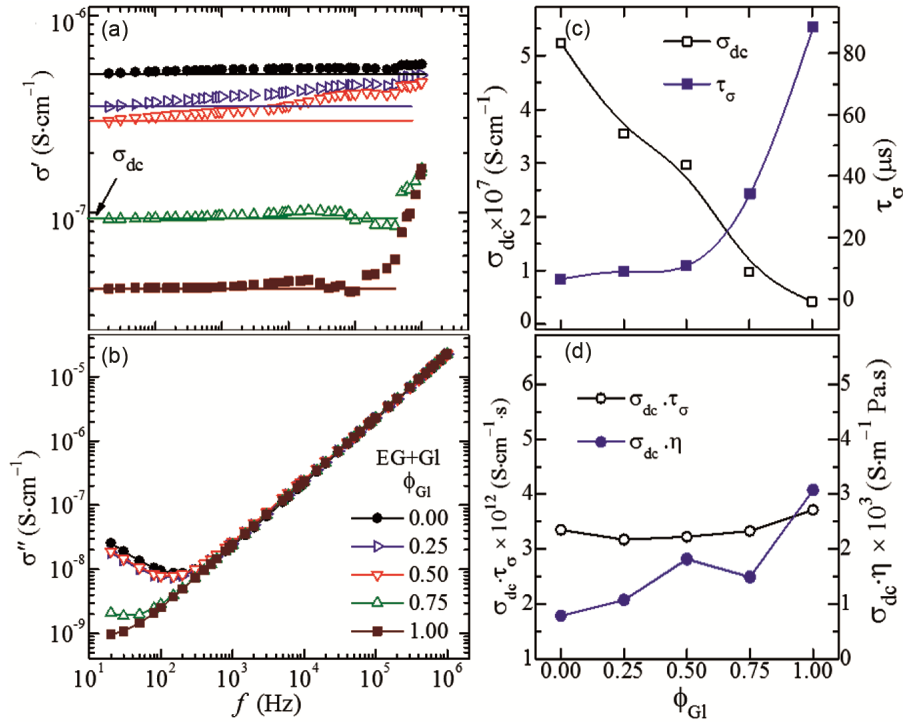
Fig. 6 — Complex ac electrical conductivity real part σ′ and σ″ imaginary part versus frequency *f* plots for the EG+Gl mixtures with different volume fraction concentrations of Gl ($\phi_{Gl}$ = 0.00, 0.25, 0.50, 0.75, and 1.00), at 298.15 K. Solid horizontal lines in (a) represent the dc electrical conductivity $\sigma_{dc}$ values on the y-axis. Plots of $\sigma_{dc}$ and $\tau_{\sigma}$ versus $\phi_{Gl}$, and the product $\sigma_{dc} \cdot \tau_{\sigma}$ and $\sigma_{dc} \cdot \eta$ versus $\phi_{Gl}$ are given in (c) and (d), respectively for the EG+Gl mixtures.

the viscosity of the dielectric medium increases. With consideration of this fact, a plot of $\sigma_{dc} \cdot \tau_{\sigma}$ product versus $\phi_{Gl}$ is given in Fig. 6(d), which shows a small change with $\phi_{Gl}$ over the entire composition range variation. This outcome evidences that the $\sigma_{dc}$ values of the EG+Gl system are predominantly ruled by the charge conductivity relaxation process. Furthermore, the $\sigma_{dc} \cdot \eta$ product versus $\phi_{Gl}$ plot depicted in Fig. 6(d), also reveals that there is an anomalous increase in the values of conductivity-viscosity product with an increase of $\phi_{Gl}$ for the EG+Gl system. This finding suggests that the $\sigma_{dc}$ values do not have a direct correlation with the η values over the entire concentration range of the EG+Gl mixtures. It may be because of the fact that there is a larger non-linear variation in the viscosities of these mixtures with concentration variation which is discussed in the latter section 3.3. Additionally, one order of magnitude variation of the $\sigma_{dc}$ values (4.2 × 10⁻⁸ to 5.23 × 10⁻⁷ S/cm) suggests that an appropriate dc conductivity liquid dielectric medium can be designed by adjusting the constituent concentration in the EG+Gl system for the electrical insulation purposes.

### 3.1.4 Complex Impedance Plots

For a dielectric medium, to understand its effective ac electrical insulation behaviour and the mechanism of charge conduction, the complex impedance function is also considered and analyzed in the previous literature[18,57,59,60,64,65]. Therefore, with this fact the *Z′* and *Z″* values of the EG+Gl binary mixtures as a function of frequency are determined from the measured $C_p$ and $R_p$ values considering the relationship given in Eq. (6)[12,64]

$$Z^*(\omega) = Z' - jZ'' = \frac{R_p}{1+(\omega C_p R_p)^2} - j\frac{\omega C_p R_p^2}{1+(\omega C_p R_p)^2} \quad \dots (6)$$

The complex impedance plane plots (*Z″* versus *Z′*) for the EG+Gl materials have appeared semicircle as given in Fig. 7. One can read from this figure that the *Z′* and *Z″* values vary in a large range with the frequency variation of the harmonic electric field and also change in the constituent concentration of these EG+Gl mixtures. The frequency values of the impedance data points are in increasing order when going from right to left with the semicircles of this figure (some frequencies are marked on the plot of the Gl material denoted by $\phi_{Gl}$ = 1). These semicircles of
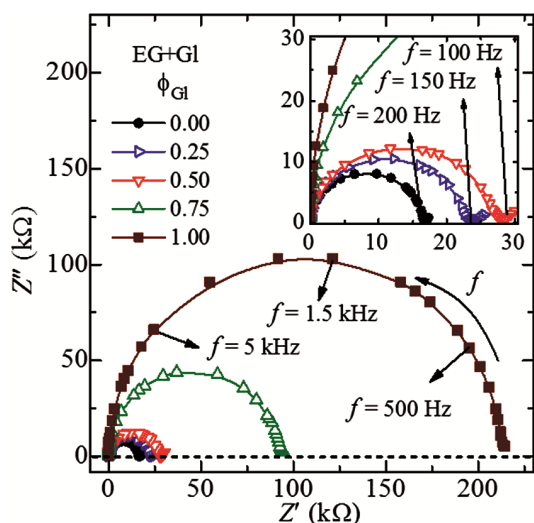
Fig. 7 — Debye plots of complex impedance $Z''$ versus $Z'$ for the EG+Gl mixtures with different volume fraction concentrations of Gl ($\phi_{Gl}$ = 0.00, 0.25, 0.50, 0.75, and 1.00), at 298.15 K. Inset shows the enlarged view of plots for the EG and EG-rich amount EG+Gl mixtures and labelled with electrode polarization relaxation process frequencies.

Fig. 8 — The plot of refractive index $n_D$ versus Gl volume fraction concentration $\phi_{Gl}$ for the EG+Gl mixtures, at 298.15 K. The dashed line represents the linear dependency and the experimental data are joined with B-spline.

impedance data plots showed the Debye-type dispersion behaviour of the EG+Gl liquid systems, and small spikes formed by the low frequency impedance data evidence the contribution of the EP effect. The frequency corresponding to the intersection point of the spike and the semicircle provides the value of electrode polarization relaxation frequency $f_{EP}$. The values of $f_{EP}$ are marked appropriately in the enlarged view of the EG-rich EG+Gl mixtures as depicted in the inset of Fig. 7. Besides this finding, the Debye semicircle of the impedance data also described the conductivity relaxation process as analyzed and demonstrated in the previous section 3.1.2 for these liquid materials from their complex electric modulus spectra. These impedance plots explain the relatively high impedance value of the Gl system and low for the EG system, and therefore, the determined $\sigma_{dc}$ values of these liquid dielectric systems are found in the inverse trend, as discussed in the previous section 3.1.3. Some characteristics like Debye semicircle, spike, intercept frequency at semicircle and spike, and dc resistance from these impedance plots of the EG+Gl system with varying constituent concentration look closely corroborated with other polar dielectric liquid systems investigated previously[11,12,14,60,64,65].

## 3.2 Refractive Indices

The refractive index $n_D$ of a polar liquid is an important physical property, and its value is
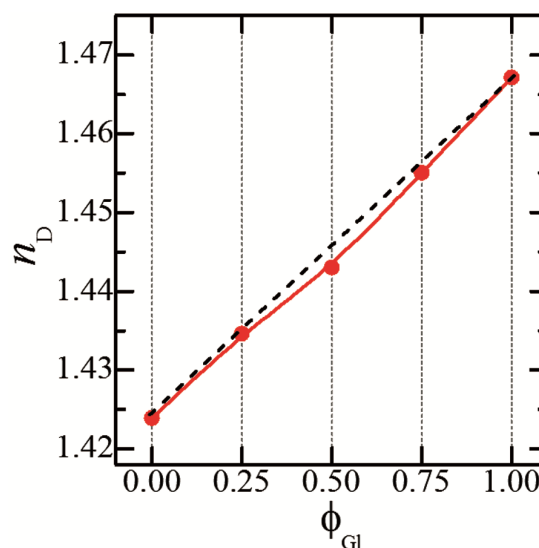
significantly affected by the nature of heterogeneous molecular interaction that takes place between the constituents of a binary mixture of polar liquids[6,11,13,16,35,46,48,55,63,66–70]. Therefore, the study of $n_D$ values with concentration variation of the EG+Gl mixtures is performed to explore the heterogeneous molecular interactions in these alcohol systems. In the case of neat liquid, the measured $n_D$ value also describes the level of purity of the material. Further, its measurement helps in the identification of a substance and specifies the dielectric and electrical response to an electric field induced by electromagnetic waves of the nanometer wavelength range[70].

The measured refractive indices of the different concentrations EG+Gl mixtures, at 298.15 K, are reported in Table 1. In Fig. 8, the variation of $n_D$ values with $\phi_{Gl}$ is presented for the EG+Gl mixtures. In comparison to the $n_D$ value of the pure EG system ($n_D$ = 1.4239), the Gl system has a significantly high $n_D$ value ($n_D$ = 1.4671), and hence, the $n_D$ values are enhanced when the $\phi_{Gl}$ values of the EG+Gl mixture were increased. Some negative deviation in the experimental $n_D$ values of the EG+Gl mixtures from the linear dependence is found in Fig. 8 which reveals some alteration in the homogeneous molecular structures of the neat EG and Gl molecules when they were mixed. It is evidence of the formation of heterogonous H-bond molecular interaction in these binary mixtures of the EG and Gl molecules which is

in agreement with the earlier results on a variety of alcohol mixtures[35]. Additionally, the deviation in refractive index values of the EG+Gl mixtures from the linearity evidence some changes in the arrangement of atoms as well as the electronic charges of the –OH functional groups of the EG and Gl molecules in their mixtures which is a result of heterogeneous molecular H-bond interaction. The high frequency limiting dielectric constant ($\varepsilon_\infty = n_D^2$) is also determined for the EG+Gl binary mixtures of different $\phi_{Gl}$ values, and the obtained $\varepsilon_\infty$ values are presented in Table 1. Using the $\varepsilon_s$ and $\varepsilon_\infty$ values, the dielectric strength $\Delta\varepsilon = \varepsilon_s - \varepsilon_\infty$ for the EG+Gl mixtures are determined and reported in Table 1, which showed an increasing behaviour (from 37.72 to 39.37) when the Gl concentration was increased.

### 3.3 Viscosities

Viscosity η values of the H-bonded polar liquids, their mixtures, and the advanced soft materials based on such liquids profoundly depend on the nature and strength of H-bond molecular interaction, and therefore, this physical property is frequently carried out for the structural conformations of a variety of liquid materials[4,12,30,40,41,52,70]. Additionally, it is a fundamental thermophysical property used in exploring the performance of heat transfer fluids in a flowing state[26,43–45]. The EG and Gl molecules have strong intermolecular H-bonding due to which their viscosities appear high to ultrahigh at ambient temperature[38,40,41,45]. It has been established that the existence of three-dimensional (3D) H-bonded molecular structures in pure Gl liquid augmented its very high viscosity as compared to the EG liquid[38,41,45]. Recently, with the consideration of ultrahigh viscosity of pure glycerol, a molecular model with supramolecular polymer structure is proposed in which the ribbon-type chains of Gl molecules are additionally linked to each other by perpendicular O-H⋯O hydrogen bonds, forming a highly arranged 3D associated molecular network[30,41]. With this fact, the addition of EG molecules in the Gl liquid is expected to modify the characteristic H-bonded 3D network of the Gl molecules.

To explore the nature of heterogeneous H-bond of EG+Gl mixtures structures and the alteration of homogeneous H-bonded structures of EG and Gl owing to heterogeneous interactions, the viscosities of these EG+Gl mixtures were measured over a wide range of shear rates, at 298.15 K. The determined viscosities of the EG+Gl mixtures, as well as that of

the pure EG and Gl systems as a function of shear rate, are depicted in Fig. 9(a). This figure, firstly, explained that the viscosities of the EG+Gl binary mixtures appeared much lower than that of the pure Gl which evidenced a large alteration in the H-bonded homogeneous structures of the Gl molecules caused by heterogeneous H-bond interactions. Secondly, the viscosity values of the neat EG, neat Gl, and their binary mixture were found independent of the shear rate which identifies these materials as Newtonian fluids which are noted consistent with several complex polar liquid materials including nanofluids[43,44]. The η values of the EG+Gl mixtures are provided in Table 1, and the neat EG and neat Gl viscosities are found in agreement with their literature values[40,41,71,72]. Besides the use of viscosity versus shear rate plots for the identification of characteristic Newtonian fluid, this behaviour can also be proved by a linear relationship obtained between the shear stress and the shear rate of the fluids[26,43,44]. The plots of
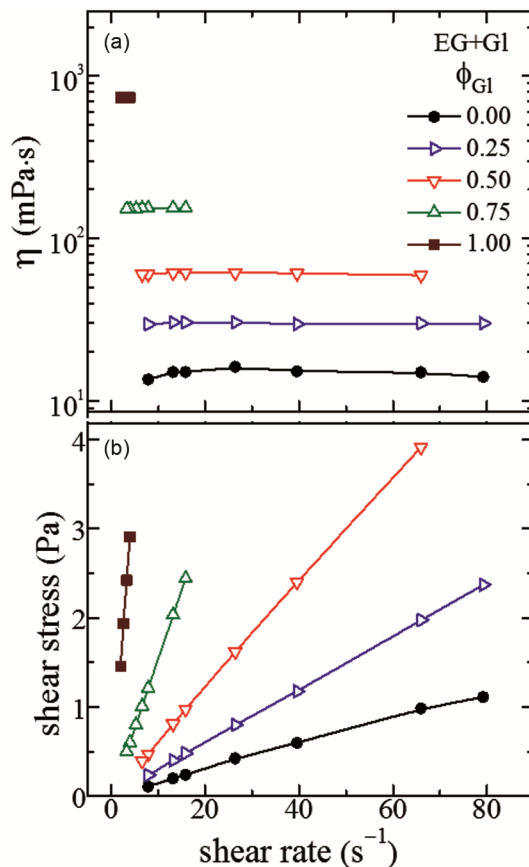


Fig. 9 — The plots of (a) viscosity η versus shear rate and (b) shear stress versus shear rate for the EG+Gl mixtures with different volume fraction concentrations of Gl ($\phi_{Gl}$ = 0.00, 0.25, 0.50, 0.75, and 1.00), at 298.15 K.

shear stress as a function of shear rate for the EG, Gl, and EG+Gl systems, at 298.15 K, are depicted in Fig. 9(b). The observed high linearity of these plots additionally confirms that the EG, Gl, and EG+Gl mixtures of all the concentrations are Newtonian fluids. Fig. 9(b) further demonstrated that the slope of the shear stress versus shear rate plots of the EG+Gl mixtures was enhanced with the increased viscosity of these Newtonian fluids.

Figure 10(a) shows the variation of viscosity on the logarithmic scale as a function of $\phi_{Gl}$ which exhibited a non-linear increase with the increase of $\phi_{Gl}$ for the EG+Gl mixtures at 298.15 K. This behaviour of viscosity reveals that the formation of heterogeneous
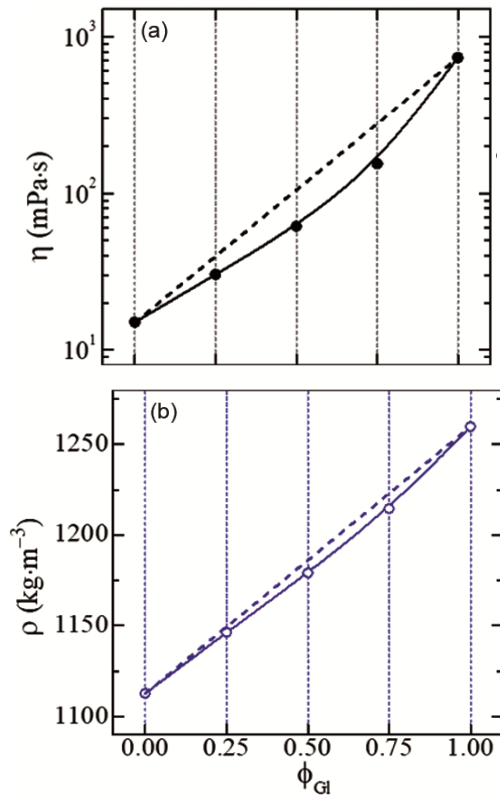


Fig. 10 — The plots of (a) viscosity η and (b) density ρ versus Gl volume fraction $\phi_{Gl}$ for the EG+Gl mixtures, at 298.15 K. The dashed lines represent linear dependency with volume fraction-weighted additivity law, and solid lines joining the experimental data points.

H-bond interactions in the EG+Gl system weakens the homogeneous intermolecular adhesion force and makes these mixtures non-ideal on the volume fraction-weighted average of the viscosity values of pure liquids. The change in two orders of magnitude in the viscosities of EG+Gl mixtures is highly appealing in regards to the design of a wide viscosity range polar solvent for the advances in fluid technologies[43,44]. The viscosity of this liquid EG+Gl mixture can be easily tuned in a wide range from 15 to 733 mPa·s, at a fixed temperature of 298.15 K, by adjusting the constituent concentration. Details with temperature variation tunable viscosity behaviour of these EG+Gl mixtures will be discussed in future works by the temperature dependent rheological measurements. The fixed temperature results of this study revealed that a suitable fluid for the pumping application needs low viscosity that can be prepared by keeping a high EG concentration in the mixture, whereas for effective load-bearing capacity purposes high viscosity fluid can be designed by taking a Gl-rich EG+Gl mixture.

**3.4 Densities**

The density ρ values of the EG, Gl, and EG+Gl systems, at 298.15 K, are listed in Table 2, and these values are also plotted against $\phi_{Gl}$ in Fig. 10(b). This figure explains the non-linear increase in ρ values with an increase of $\phi_{Gl}$ in the EG+Gl mixtures, which is primarily due to the higher density of the neat Gl liquid. The deviation of these mixture densities from the linear dependences can be noted in this figure which infers the formation of heterogeneous H-bond interactions between the EG and Gl molecules as concluded for several other binary polar liquid mixtures[4,6,9,16,25,52,54,55,66–68]. Further, the ρ values of these EG+Gl mixtures are observed slightly lower than their linear dependency behaviour.

The reduction of density values from the ideal linearity is presumably the interpenetration of the EG molecules in the tightly H-bonded connected homogeneous 3D network of the Gl molecules.

Table 2 — The values of density ρ, ultrasound velocity $u$, adiabatic compressibility $\beta_a$, intermolecular free length $L_f$, acoustic impedance $Z_a$, and thermal conductivity $k$ for binary mixtures of EG+Gl with varying Gl volume fraction concentration $\phi_{Gl}$, at 298.15 K.

| $\phi_{Gl}$ | $\rho$ (kg·m$^{-3}$) | $u$ (m·s$^{-1}$) | $\beta_a \times 10^{10}$ (m$^2$·N$^{-1}$) | $L_f \times 10^{11}$ (m) | $Z_a \times 10^{-6}$ (kg·m$^{-2}$·s$^{-1}$) | $k$ (W·m$^{-1}$·K$^{-1}$) |
|---|---|---|---|---|---|---|
| 0.00 | 1112.7 | 1655 | 3.28 | 3.73 | 1.84 | 0.3124 |
| 0.25 | 1146.3 | 1710 | 2.98 | 3.55 | 1.96 | 0.3095 |
| 0.50 | 1179.1 | 1778 | 2.68 | 3.37 | 2.10 | 0.3075 |
| 0.75 | 1214.5 | 1834 | 2.45 | 3.22 | 2.23 | 0.3026 |
| 1.00 | 1259.7 | 1920 | 2.15 | 3.02 | 2.42 | 0.3028 |

This type of mixing arrangement at the molecular level causes broken of some homogeneous H-bonded structures and relatively loosens the formed heterogeneous molecular networks of the EG+Gl system. Because of this fact, there is a creation of some additional free volume in the mixed system of the EG and Gl molecules as compared to that of the pure Gl network molecular packing at 298.15 K. This argument also favours the lowering in the viscosity of the EG+Gl mixture from the ideal-mixture behaviour as explained in previous section 3.3.

**3.5 Ultrasound Velocities and Acoustic Parameters**

Ultrasound wave velocity $u$ is highly sensitive to the molecular structure and its study on a liquid system can be utilized to explain the molecular interactions present in the liquid system. It is because of the fact that the experimental $u$ values have a direct correlation with the binding forces that exist between the neighbouring molecules in a homogeneous system and also the components molecules of a binary mixture[6,9,16,25,50–56,66–68,73]. Therefore, the study of $u$ values is considered an important experimental approach to exploring the nature of H-bonded molecular interactions and also identification of heterogeneous structures in a variety of liquid mixtures[6,9,16,52–55,66–68]. The $u$ value of a liquid system is governed both by the elastic property (rigidity or stiffness) and the inertial property (the mass density of individual constituents in the complex liquid medium). Therefore, the measurement of $u$ value has significance in the determination of several important acoustical and thermophysical parameters of a liquid system for the confirmation of different industrial uses. The most usable acoustic parameters of liquid material are the adiabatic compressibility, intermolecular free length, acoustic impedance, and thermal conductivity. These parameters are briefly explained for the interest of readers herein to understand their dependency on $u$ values and some other thermodynamical quantities, which altogether can provide better insight into the molecular structure of a complex fluid system as utilized in the previous literature[6,9,16,50–55,66,73–75].

The adiabatic compressibility $\beta_a$ determines the structural arrangement and orientation of molecules in a liquid system when the molecules of such system are stimulated by delivering the mechanical energy (pressure vibrations) of an ultrasonic wave[73,75]. The $\beta_a$ value of a simple liquid and also a complex fluid is determined from the experimental $u$ and $\rho$ values

using the Newton-Laplace relationship given in Eq. (7) and it is used earlier in several researches[6,9,25,50,64,66,67,75];

$$\beta_a = 1/\rho u^2 \qquad \qquad \ldots (7)$$

The intermolecular free length $L_f$ is an important physical property that is a measure of the average distance between the molecular surfaces of neighbouring molecules in a liquid and liquid mixture, and it can be calculated from the $\beta_a$ based relationship printed as Eq. (8)[9,25,51,54,55,67,76];

$$L_f = K_T (\beta_a)^{1/2} \qquad \qquad \ldots (8)$$

Where $K_T$ is Jacobson's constant[77] and it has the temperature $T$ dependent numerical value that can be determined from the relationship $K_T = (93.875 + 0.375T) \times 10^{-8}$ kg$^{1/2}$·m$^{1/2}$·s$^{-1}$ [9,25,77,78].

The determination of acoustic impedance $Z_a$ signifies the behaviour of ultrasound wave transmission and reflection in a liquid medium. The $Z_a$ of a liquid system has a proportionality relationship both with the $\rho$ and $u$ according to Eq. (9)[25,50,51,55,67,68,76];

$$Z_a = \rho u \qquad \qquad \ldots (9)$$

The thermal conductivity $k$ determination provides the appropriateness of a fluid or nanofluid to be used in a variety of heat transfer systems[10,26,43,79]. Initially, Bridgman[80] established a relationship between ultrasound velocity $u$ and thermal conductivity $k$ of a liquid system which was later modified taking its numerical coefficient value 2.8 instead of 3 for better agreement of other techniques experimental data[81,82]. This relationship is given in Eq. (10) and is frequently used for the study of $k$ values of the nanofluids[30,32,76,79];

$$k = 2.8 \, u \, (N/V)^{2/3} K_B \qquad \qquad \ldots (10)$$

Where $N$ is the Avogadro number, $V$ is the molar volume of the liquid system related to the molar mass $M$ and the density $\rho$ given by $V = M/\rho$, and $K_B$ is the Boltzmann's constant. The experimental values of $u$ and $\rho$ along with the computed values of $\beta_a$, $L_f$, $Z_a$, and $k$ for the EG, Gl, and EG+Gl mixtures at 298.15 K are reported in Table 2.

Furthermore, the determinations of Rao's constant $R_i$ (*i.e.*, molar sound velocity)[83] given by Eq. (11) and Wada's constant $W$ (*i.e.*, molecular compressibility)[84] from Eq. (12), which are based on experimental data of $u$ and $\rho$, have significance to describe the strength of molecular interaction and density of hydrogen bonds in a complex liquid system[9,50,54,68,76];

$$R_i = (M/\rho)\, u^{1/3} \qquad \ldots (11)$$

$$W = (M/\rho)\, \beta_a^{-1/7} \qquad \ldots (12)$$

The molecular vibrational dynamics in a viscous liquid under the influence of longitudinal ultrasound waves can be explained with the determination of molecular viscoacoustic relaxation time $\tau_{\eta a}$[25,67]. The $\tau_{\eta a}$ value is a measure of time taken for the excitation energy to appear as translational energy in a homogeneous or heterogeneous liquid system. Considering the experimental data of $\eta$, $\rho$, and $u$, of a liquid system, the $\tau_{\eta a}$ value can be calculated employing Eq. (13) given in the literature[25,67,85];

$$\tau_{\eta a} = (4\eta/(3\rho u^2)) = (4/3)\,\eta\beta_a \qquad \ldots (13)$$

The study of free volume $V_f$ of a liquid mixture is one of the significant physical factors in explaining the molecular structural arrangement. Furthermore, the physicochemical behaviour with the variation in constituents concentrations of a mixed liquid, at a fixed temperature, can be explored from the $V_f$ data. The $V_f$ value is mainly ruled by the molecular structure like the size and shape of the molecules, and the nature of intermolecular interactions. The molecular interactions in the liquid state did not bear enough strength to pack the molecules tightly and also hold them closely in the thermodynamic equilibrium, and therefore there is always the existence of some vacant space between them. This vacant space between the individual molecules and their associated clusters is defined as free volume. Eyring and Kincaid[86] explained that the $V_f$ value of a liquid system can be determined by taking the total integral over that part of the potential energy which is due to the thermal displacement of the centre of gravity of the molecule from the equilibrium position. In the case of EG+Gl mixture the displacement of the centre of gravity of the molecule, at a fixed temperature, is attributed to the H-bond heterogeneous interaction. A relationship of $V_f$ with the $M$, $u$, and $\eta$ for a liquid system is presented in Eq. (14) which is frequently used for the study of molecular interaction in liquid mixtures[25,54,76,85];

$$V_f = (Mu/K\eta)^{3/2} \qquad \ldots (14)$$

Where $K$ is a temperature independent constant of numerical value $4.28 \times 10^9$ mol$^{-1/3}$ for the liquid systems. The values of $R_i$, $W$, $\tau_{\eta a}$, and $V_f$ computed for the EG, Gl, and EG+Gl mixtures, at 298.15 K, are listed in Table 3.

To understand more about the nature of H-bonded heterogeneous interaction of the EG molecules with the Gl molecules in the EG+Gl mixtures, the values of $u$, $\beta_a$, $L_f$, $Z_a$, $k$, $R_i$, $W$, $\tau_{\eta a}$, and $V_f$ of these mixtures are plotted against $\phi_{Gl}$ in Fig. 11(a–i). From these plots, the deviation of various parameters experimental values from the linear dependency is identified and considered to explain the strength of heterogeneous molecular interactions in the EG+Gl mixtures. The deviation values of these acoustic parameters of the EG+Gl mixtures are herein denoted by $\delta u$, $\delta Z_a$, $\delta k$, $\delta R_i$, $\delta W$, $\delta \tau_{\eta a}$, and $\delta V_f$ and the same are reported in Table 4 which may be interesting for the readers. Fig. 11(a) shows that the $u$ values of EG+Gl mixtures increase with an increase of $\phi_{Gl}$, which is owing to the high $\eta$ value of the Gl system as well as its high density as compared to that of the EG system. It can be noted from this figure that the $u$ values of the EG+Gl mixtures are lower than the linear dependence behaviour. This outcome evidences that the EG and Gl heterogeneous H-bonded molecular structures make slow down the propagation of the acoustic wave in these mixtures. The $\delta u$ value is noted as maximum (20.9 m·s$^{-1}$) at $\phi_{Gl} = 0.75$ for these EG+Gl mixtures (see Table 4) confirming more influence of heterogeneous interaction on the propagation of the acoustic wave in Gl-rich mixture.

Figures 11(b) & 11(c) reveal that the $\beta_a$ and $L_f$ decreased linearly when the $\phi_{Gl}$ was increased in the EG+Gl binary mixtures. Further, the deviation in these parameters from the linear behaviour is not noticeable. Therefore, the explanation of heterogeneous interactions using the $\beta_a$ and $L_f$ versus $\phi_{Gl}$ plots is not found appropriate for the EG+Gl mixtures. It seems that the factors which influence the compressibility and intermolecular free length are balanced in such a manner that they compensate for the overall effect of the interaction with constituents

Table 3 — The values of Rao constant $R_i$, Wada constant $W$, viscoacoustic relaxation time $\tau_{\eta a}$, and free volume $V_f$ for the binary mixtures of EG+Gl with varying Gl volume fraction concentration $\phi_{Gl}$, at 298.15 K.

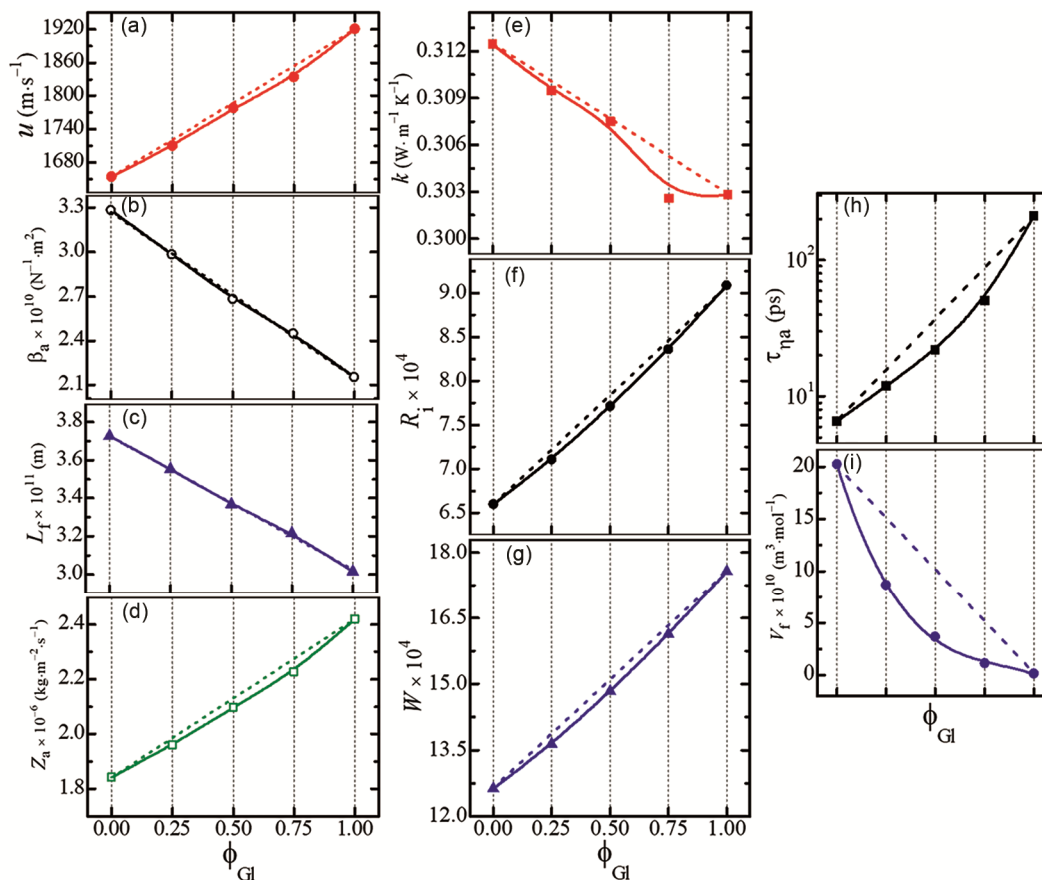| Acoustic parameters | $\phi_{Gl}$ | | | | |
|---|---|---|---|---|---|
| | 0.00 | 0.25 | 0.50 | 0.75 | 1.00 |
| $R_i \times 10^4$ (m$^3$·mol$^{-1}$·m$^{1/3}$·s$^{-1/3}$) | 6.6 | 7.1 | 7.7 | 8.4 | 9.1 |
| $W \times 10^4$ (m$^3$·mol$^{-1}$ (kg$^{-1}$·m·s$^2$)$^{-1/7}$) | 12.6 | 13.6 | 14.8 | 16.1 | 17.6 |
| $\tau_{\eta a} \times 10^{12}$ (s) | 6.6 | 11.9 | 21.8 | 50.3 | 210.4 |
| $V_f \times 10^{10}$ (m$^3$·mol$^{-1}$) | 20.23 | 8.65 | 3.65 | 1.11 | 0.13 |

Fig. 11 — The plots of (a) ultrasonic velocity $u$, (b) adiabatic compressibility $\beta_a$, (c) intermolecular free length $L_f$, (d) acoustical impedance $Z_a$, (e) thermal conductivity $k$, (f) Rao constant $R_i$/ $m^3 \cdot mol^{-1} \cdot m^{1/3} \cdot s^{-1/3}$, (g) Wada constant $W$/ $m^3 \cdot mol^{-1}(kg^{-1} \cdot m \cdot s^2)^{-1/7}$, (h) viscoacoustic relaxation time $\tau_{\eta a}$, and (i) free volume $V_f$ versus the Gl volume fraction concentrations $\phi_{Gl}$ for the EG+Gl mixtures at 298.15 K. Dashed straight lines drawn with these pots represent the linear dependency of these parameters based on volume fraction-weighted additivity law and solid lines join the experimental data points.

Table 4 — The magnitude of deviation values of ultrasound velocity $\delta u$, acoustic impedance $\delta Z_a$, thermal conductivity $\delta k$, Rao constant $\delta R_i$, Wada constant $\delta W$, viscoacoustic relaxation time $\delta \tau_{\eta a}$, and free volume $\delta V_f$ for the binary mixtures of EG+Gl mixtures with varying Gl volume fraction concentration $\phi_{Gl}$, at 298.15 K

| $\phi_{Gl}$ | $\delta u$ (m·s$^{-1}$) | $\delta Z_a \times 10^{-6}$ (kg·m$^{-2}$·s$^{-1}$) | $\delta k \times 10^4$ (W·m$^{-1}$·K$^{-1}$) | $\delta R_i \times 10^4$ (m$^3$·mol$^{-1}$·m$^{1/3}$·s$^{-1/3}$) | $\delta W \times 10^4$ (m$^3$·mol$^{-1}$(kg$^{-1}$·m·s$^2$)$^{-1/7}$) | $\delta \tau_{\eta a} \times 10^{12}$ (s) | $\delta V_f \times 10^{10}$ (m$^3$·mol$^{-1}$) |
|---|---|---|---|---|---|---|---|
| 0.25 | 11 | 0.025 | 6.00 | 0.10 | 0.269 | 3.84 | 6.51 |
| 0.50 | 8.1 | 0.034 | 1.90 | 0.13 | 0.290 | 15.2 | 6.49 |
| 0.75 | 20.9 | 0.047 | 26.8 | 0.097 | 0.220 | 37.4 | 3.98 |

volume-fraction concentration variation in the EG+Gl mixtures. But a significant lowering of $Z_a$ values from the linearity for the EG+Gl mixtures can be seen in Fig. 11(d) which also confirms the formation of heterogeneous H-bonding between the EG and Gl molecules in their mixture. Similar to the maximum $\delta u$ value, the maximum $\delta Z_a$ also appeared for the Gl-rich this binary mixture (see Table 4).

A plot of $k$ versus $\phi_{Gl}$ for the EG+Gl binary mixture is shown in Fig. 11(e) which illustrates that the $k$ values of these mixtures decrease with the

increase of $\phi_{Gl}$, except the binary mixture having $\phi_{Gl}$ value of 0.75 for which the $k$ value is noted close to that of the pure Gl liquid. The $k$ values of pure EG and pure Gl fluids determined in this study are noted as slightly higher than that of their literature values obtained by the transient hot-wire method[26,29,39,45]. This finding suggests that the determination of thermal conductivity using ultrasound velocity based Eq. (10) needs some additional correction at every concentration of these highly viscous heterogeneous H-bonded EG+Gl mixtures. A correction constant was

also applied earlier for the EG-based nanofluids to get the correct $k$ value from Eq. (10)[32], but this relation was found appropriate for the thermal conductivity study of water and its based nanofluids[79].

The values of Rao's constant $R_i$ and Wada's constant $W$ for the EG+Gl mixtures also exhibited some deviation from the linear dependency (see Figs. 11(f) & 11(g)). Earlier, it is demonstrated that the linear dependence of the $R_i$ and $W$ on the concentration of binary liquid mixtures is exhibited only when the complexes or heterogeneous interactions are either not formed or are very weak[9,55,68]. But the significant $\delta R_i$ and $\delta W$ values of the EG+Gl mixtures (Table 4) confirm that the H-bond heterogeneous interactions are formed in the studied systems which are consistent with the results on other liquids mixtures[50,54,68].

Figures 11(h) & 11(i) illustrate the variation of $\tau_{\eta a}$ and $V_f$ values with $\phi_{Gl}$ for the EG+Gl mixtures at 298.15 K. As expected from Eq. (13), owing to the high viscosity of pure Gl, the $\tau_{\eta a}$ values enhance with the increase of $\phi_{Gl}$ for the EG+Gl mixtures. But the observed non-linear increase of $\tau_{\eta a}$ (a significant deviation of $\delta\tau_{\eta a}$ from the linear dependence, see Table 4) also confirms the formation of H-bonding between the EG and Gl molecules with a simultaneous breaking of some homogeneous H-bonded networks of these molecules. Similar to the $\delta u$, and $\delta Z_a$ values, the $\delta\tau_{\eta a}$ value is found maximum (37.4 ps) at $\phi_{Gl} = 0.75$ for the EG+Gl mixture. In contrast to the increasing behaviour of $\tau_{\eta a}$, the $V_f$ values decrease when the $\phi_{Gl}$ increases in the EG+Gl mixtures. A relatively high $V_f$ value of the EG system reveals lesser packing of the EG molecules through H-bonding in its pure state as compared to the strong 3D H-bonding of the Gl molecules. This observation also supports the appeared relatively high values of the Kirkwood correlation factor of the neat Gl system, reported in the literature[38,41]. Significant values of $\delta V_f$ for the EG+Gl mixtures (Table 4) favours the formation of an H-bonded heterogeneous network at all the concentrations of the mixtures.

### 3.6 Excess Parameters

The experimental values of some of the thermodynamic parameters that exhibited non-linear behaviour with $\phi_{Gl}$ for the EG+Gl mixtures, as discussed in the previous sections, are now considered for the determination of their excess values in order to better understand the heterogeneous

molecular H-bonding in these mixtures. It is interesting because of the fact that the study of excess properties is recognized as more meaningful and authentication in exploring the heterogeneous interactions and formation of some stable moieties in the mixed solvents[1,6–9,11–14,16,20,21,40,46–49,53,69,87]. The excess static dielectric permittivity $\varepsilon_s^E$, excess refractive index $n_D^E$, excess viscosity $\eta^E$, excess ultrasound velocity $u^E$, excess viscoacoustic relaxation time $\tau_{\eta a}^E$, excess acoustic impedance $Z_a^E$, and excess free volume $V_f^E$ values for the EG+Gl binary mixtures are determined, at 298.15 K, by using the mixture constituents volume fraction-weighted additivity relation as well as mole fraction-weighted additivity relation. Generalized expression for the excess parameters $Y^E$ for the EG+Gl binary mixtures, can be defined by Eq. (15);

$$Y^E = Y_m - \left( a_{EG}\, Y_{EG} + a_{Gl}\, Y_{Gl} \right) = Y_m - Y^{id} \quad \dots (15)$$

Where $Y_m$, $Y_{EG}$, and $Y_{Gl}$ refer to the measured values of various parameters such as $\varepsilon_s$, $n_D$, $\eta$, $u$, $\tau_{\eta a}$, $Z_a$, and $V_f$ of the EG+Gl mixture, pure EG, and pure Gl, respectively. The $a_{EG}$ and $a_{Gl}$ are either the volume fractions $\phi$ or the mole fraction $x$ of the EG and Gl, respectively, in the EG+Gl mixture. The term printed in the bracket on the right side of Eq. (15) represents the ideal mixture thermodynamic property $Y^{id}$ at the same temperature and pressure at which measured for the mixture. Although, there is still controversy on the use of volume fraction-weighted additivity or mole fraction-weighted additivity law in regards to thermodynamical parameters ideality of the binary mixtures. Nevertheless, for the determination of $\varepsilon_s^E$ values, the use of the volume fraction-weighted additivity law is well demonstrated[21,48,63,66,87]. For the $n_D^E$ values, both volume fraction and mole fraction-weighted additivity laws are demonstrated in different researches[6,48,51,55,69]. Many researchers used the mole fraction-weighted additivity law for the determination of $\eta^E$ values of the liquid mixtures and also some of the excess acoustic parameters[25,55,66,88,89]. With the consideration of these facts, herein, we determined the values of various excess parameters by using volume fraction as well as mole fraction additivity laws for the EG+Gl mixtures for better structural

understanding and the benefit to the readers. The computed excess values of different parameters as a function of $\phi_{Gl}$ as well as $x_{Gl}$ for the EG+Gl mixtures, at 298.15 K, are plotted in Fig. 12. These plots are for the nature of heterogeneous H-bond interactions and probable stable moieties in the EG+Gl mixtures.

Figure 12 demonstrates that the $\varepsilon_s^E$ values of the EG+Gl mixtures are positive whereas $\eta^E$, $\tau_{\eta a}^E$, and $V_f^E$ values are negative and exhibited almost identical behaviour on the volume fraction $\phi_{Gl}$ and mole fraction $x_{Gl}$ scales. These excess values of various parameters evidence the presence of heterogeneous H-bonded structures of unlike molecules in the formulated EG+Gl mixtures. The positive $\varepsilon_s^E$ values (Fig. 12(a)) confirm the increase in the number of effective dipoles aligned in the same direction as a result of H-bond formation between the EG and Gl molecules in their mixtures. In contrast to the positive $\varepsilon_s^E$ values, the $n_D^E$ values are negative with volume

fraction and exhibited anomalous changes with the mole fraction of the mixtures (Fig. 12(c)). These $n_D^E$ values evidence that there is a disturbance in the arrangement of atomic charges, especially of the –OH functional groups of the EG and Gl molecules in the EG+Gl mixtures which are owing to the H-bond heterogeneous interactions.

The study of $\eta^E$ values provides information about the nature of heterogeneous intermolecular interaction in polar liquid mixtures. The positive $\eta^E$ values evidenced a complex formation due to specific interactions whereas the negative values of the different molecule sizes containing binary mixtures identify the dominance of homogenous molecular forces in the mixtures[12,14,40,70,89]. For the EG+Gl mixtures, the $\eta^E$ values are negative as seen in Fig. 12(b) which infers that there is a break in some homogeneous H-bonded 3D molecular networks of the Gl molecules caused by the formation of
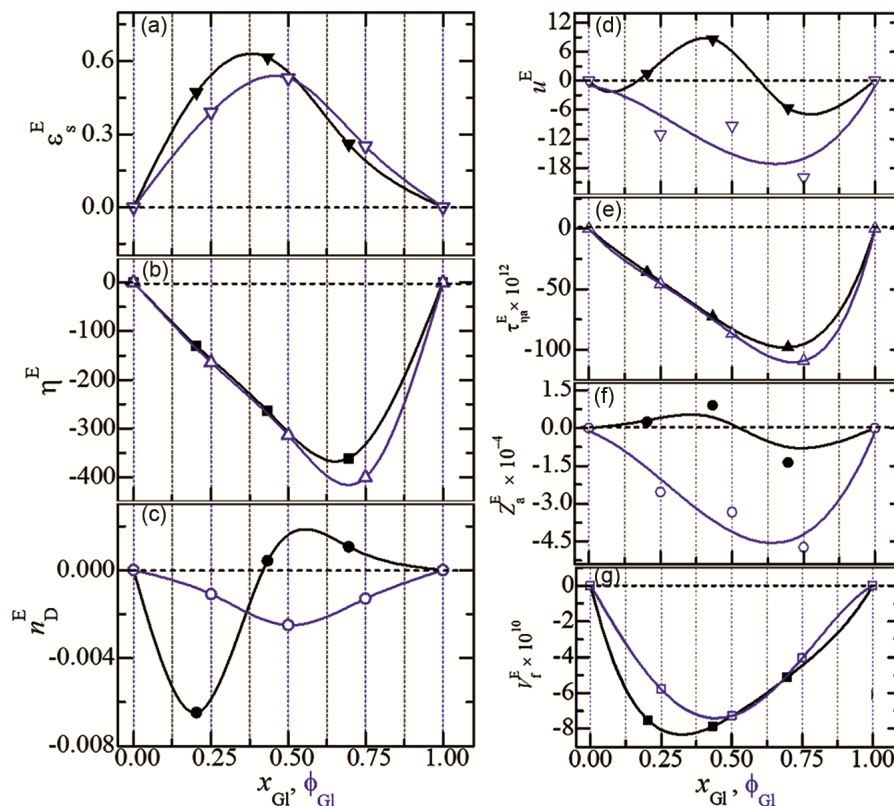


Fig. 12 — The plots of (a) excess static dielectric permittivity $\varepsilon_s^E$, (b) excess viscosity $\eta^E$ / mPa·s, (c) excess refractive index $n_D^E$, (d) excess ultrasound velocity $u^E$ / m·s$^{-1}$, (e) excess viscoacoustic relaxation time $\tau_{\eta a}^E$ / s, (f) excess acoustic impedance $Z_a^E$ / kg·m$^{-2}$·s$^{-1}$, and (g) excess free volume $V_f^E$ / m$^3$·mol$^{-1}$ versus Gl volume fraction concentration $\phi_{Gl}$ (unfilled blue colour symbols) as well as mole fraction concentration $x_{Gl}$ (filled black colour symbols) for the EG+Gl mixtures, at 298.15 K.

heterogeneous H-bonds networks with the EG molecules. A similar type of behaviour was also explained for other binary mixtures of associating molecules[40,88]. The $u^E$ and $Z_a^E$ values of these EG+Gl mixtures are also reported in Fig. 12 (d) & (f) for understanding their variation. The observed negative $\tau_{\eta a}^E$ values of the EG+Gl mixtures (Fig. 12(e)) show an enhancement in the dynamics of EG and Gl molecules within their H-bonded heterogeneous molecular networks. The plots of negative $V_f^E$ values with both the $x_{Gl}$ and $\phi_{Gl}$ for the EG+Gl mixtures (Fig. 12(g)) showed close resemblance and also confirm the formation of heterogeneous molecular interaction between the EG and Gl molecules. Furthermore, the constituents concentration corresponding to the maximum magnitude of excess parameters values represents a relatively stable moiety of the H-bonded EG and Gl molecules in the formulated EG+Gl mixtures. The various parameters excess properties plots shown in Fig. 12 identify the mixtures of EG:Gl with stoichiometric ratios of 1:1 and 3:1 for the stable moieties.

### 3.7 Ultraviolet-Visible (UV-Vis) Spectra

The UV-Vis absorbance study is meaningful for confirmation of heterogeneous molecular interaction in the liquid mixtures and also the characteristic complexes formed in the hybrid

liquid systems[4,24,31,45,70,90–94]. The absorbance spectra measured in the wavelength $\lambda$ range from 200 nm to 1100 nm for the pure EG, pure Gl, and also the varying concentration EG+Gl mixtures are depicted in Fig. 13. As can be seen from this figure that all these liquid systems are highly transparent (no absorbance) in the entire visible range. This evidences that the energies of the visible range photons are insufficient to excite the auxochrome (the lone electrons pairs of the hydroxyl oxygen atoms) of the EG and Gl molecules in a pure liquid state as well as their binary mixtures. A gradual increase in absorbance for these liquid systems is noted in the UV region when the incident radiation $\lambda$ decreases below 350 nm. With decreasing the wavelength of UV-radiations, initially weak but sharp absorbance bands have appeared at 269 nm and 262 nm for the pure EG and the EG+Gl mixtures which represent two discrete secondary transitions in these systems, whereas pure Gl showed a very weak and broader hump centered around 270 nm confirming insignificant secondary transition (see enlarged view in Fig. 13(b). Further, it can be seen from Fig. 13(b) that both the secondary transitions absorbance peak positions (marked with vertical dashed lines) are independent of these mixture constituents concentration. But peak intensities of these bands reduce with the increase of Gl concentration $\phi_{Gl}$ (from 0.00 to 0.75) suggesting that
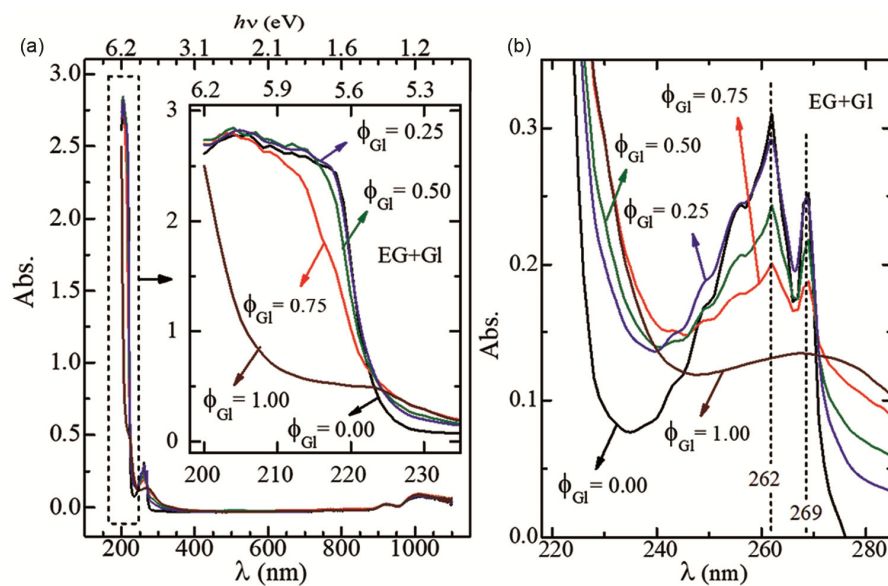


Fig. 13 — Plots of (a) absorbance (Abs.) versus wavelength $\lambda$ and photons energy $h\nu$ for the EG+Gl mixtures with different volume fraction concentrations of Gl ($\phi_{Gl}$ = 0.00, 0.25, 0.50, 0.75, and 1.00), at ambient temperature. The enlarged view in inset (a) shows the useful part of the spectra from the 200 nm to 235 nm range that represents the main absorbance band and in (b) the enlarged view of the weak bands labelled with their peaks by vertical dashed lines.

the secondary transitions in EG+Gl mixtures are ruled by the hypochromic effect. The changes in intensities of these bands also reveal a decrease in the number of H-bond associated heterogeneous structures of the EG and Gl molecules in the EG+Gl mixtures which supports the structural findings of these mixtures from the analysis of their dielectric properties.

With the further decrease of wavelength in the UV region below 240 nm, a relatively strong absorbance appeared corresponding to a primary electronic transition of the EG+Gl liquid materials which also represents a collective transition. The inset of Fig. 13(a) explains that the onset wavelength corresponding to a sharp rise in absorbance band is about 225 nm for the pure EG liquid and also the EG+Gl mixtures whereas it is around 210 nm for the pure Gl liquid. It is also noted from the inset of Fig. 13(a) that the primary band of Gl remains merged with that of the EG band when there is an increase of $\phi_{Gl}$ up to 0.50. The earlier studies concluded that the molecular interactions in a mixture of two distinct chromophores or auxochromes containing molecules can be analyzed from UV-Vis spectra by relative changes in the position and intensity of the bands associated with the chromophores[70,91,94,95]. But the exhibited distinct bands in a mixture of different molecules having the same chromophores or auxochromes primarily identify the heterogeneous molecular interaction[70], as it is noted in the present study on the EG+Gl mixtures. Some of these interpretations related to heterogeneous molecular association and dipolar orientation in different binary mixtures are also found consistent with the previous results demonstrated by simultaneous analysis of their dielectric properties and the UV-Vis spectra[92,93,96].

The photons energies corresponding to secondary absorbance bands peaks of 269 nm and 262 nm for the EG system as well as the EG+Gl mixtures are 4.61 eV and 4.73 eV, respectively. The primary absorbance band photons energies for the electronic excitation of lone electrons pairs of the hydroxyl oxygen atoms (n $\rightarrow$ $\sigma^*$ transition) of the EG and the EG-rich EG+Gl mixtures is about 5.51 eV, whereas it is 5.90 eV for the pure Gl. But the Gl-rich EG+Gl mixture of $\phi_{Gl}$ = 0.75 has an energy value slightly higher than that of the EG system. These results are attributed to the strength of like molecules H-bond interactions in the pure liquids and the unlike molecules interaction in the mixed liquids of the EG and Gl. The higher electronic transition energy for the

pure Gl liquid evidences stronger H-bond homogeneous molecular interactions in this system while these interactions seem relatively less strong between the EG molecules as revealed from its slightly low energy which also favours the explanations made on the behaviour of molecular interactions in these systems with the consideration of their values of Kirkwood correlation factor[38].

A redshift of 15 nm in the absorbance band for the Gl-rich EG+Gl mixture (*i.e.*, at 225 nm) as compared to the band position of pure Gl (i.e., 210 nm) confirms the formation of heterogeneous H-bond interaction of the EG and Gl molecules. Additionally, the transition energies of other concentration EG+Gl mixtures noted close to that of the pure EG evidence the existence of heterogeneous H-bond molecular interactions but it seems that there is no more alteration in the arrangement of electronic charges of the –OH functional group. Some of the UV-Vis results on these EG+Gl mixtures bearing the hydroxyl functional group constituents are found meaningfully consistent with the liquid mixtures containing one of the constituents with a hydroxyl group and the other constituent of the different functional group[4,91,94].

## 4 Conclusions

This paper reports the complex dielectric permittivity spectra of the pure EG, pure Gl, and the EG+Gl mixtures, at 298.15 K as well as the electric modulus, ac electrical conductivity, and impedance spectra over the static permittivity frequency regime from 20 Hz to 1 MHz and their detailed analysis regarding the low frequency dielectric dispersion behaviour and dielectric parameters of these liquid systems. The variation in the values of static dielectric permittivity, relaxation times for the electrode polarization and the charge conductivity processes, and also the dc electrical conductivity with the change in constituent concentration of the EG+Gl mixtures evidenced the alteration in H-bonded homogeneous molecular structures and simultaneous formation of heterogeneous structures with the increased dipole ordering and the facilitated dynamical processes. Refractive index, viscosity, density, ultrasound wave velocity, viscoacoustic relaxation time, free volume, and acoustic impedance values of the EG+Gl mixtures over the entire composition range are reported. The excess values of dielectric, electrical, and some thermophysical parameters confirmed the formation of heterogeneous hydrogen-bonded molecular structures with the 1:1 and 3:1 stoichiometric ratio

stable moieties in these EG+Gl mixtures. The H-bond interactions formed between the EG and Gl molecules were also confirmed by the analysis of relative changes either in intensity or position of the primary and secondary transition absorbance bands in the UV region. The energy values related to these electronic transitions of lone electron pairs of hydroxyl oxygen atoms are also reported for the EG+Gl systems. The H-bond heterogeneous interaction behaviour of the EG and Gl molecules in their mixtures was thoroughly characterized by multiphysics approaches which are its kind of first and in-depth study on the highly complex mixtures of associating molecules.

The EG+Gl mixtures have high dielectric strength, appreciable low dc electrical conductivity, wider viscosity range, a significant adjustable ultrasound velocity as well as thermal conductivity, and also some controllable behaviour of the optical parameters which all together reveal that these liquid materials are potential candidates for a wide range of industrial and technological applications. Additionally, the green, non-toxic, and biodegradable characteristics of the EG+Gl mixtures confirm their appropriateness, especially as a tunable mixed solvent for the execution of various chemical, biological, and pharmaceutical processes, and also as novel green fluids for energy transportation in all advanced heating as well as cooling systems. Such detailed findings with multiphysics experimental approaches open an important avenue for the characterization of various mixed solvents concerning the advances in science and engineering of next-generation soft condensed materials-based technologies.

## Acknowledgements

## References

1   Mehrotra S C, Kumbharkhane A C & Chaudhari A, Elsevier Science Publishing Co. Inc, Cambridge, (2017).

2   Sudo S, Shinyashiki N, Kitsuki Y & Yagihara S, *J Phys Chem A*, 106 (2002) 458.

3   Rana V A, Shah N S, Shah K N & Vankar H P, *J Mol Liq*, 369 (2023) 120829.

4   Saknure S H, Garad N P, Gubre A G, Joshi Y S & Kumbharkhane A C, *Indian J Pure Appl Phys*, 61 (2023) 27.

5   Jia G Z, Jie Q & Feng W, *J Mol Struct*, 1100 (2015) 354.

6   Chęcińska-Majak D, Klimaszewski K, Stańczyk M, Bald A, Sengwa R J & Choudhary S, *J Chem Thermodyn*, 102 (2016) 164.

7   Manjula V, Prasad T V, Balakrishna K, Raju K C J & Vishwam T, *J Mol Struct*, 1227 (2021) 129703.

8   Senthilkumar P, Saravanakannan V, M Sylvester M, Vinoth K, Deshmukh A R, Ganesh T & Kumbharkhane A C, *J Mol Liq*, 372 (2023) 121129.

9   Mozo I, González J A, Fuente I G de la, Cobos J C & Riesco N, *J Mol Liq*, 140 (2008). 87.

10   Liu C, Qiao Y, Lv B, Zhang T & Rao Z, *Int Commun Heat Mass Transf*, 112 (2020) 104491.

11   Vankar H P & Rana V A, *J Mol Liq*, 254 (2018) 216.

12   Sengwa R J, Choudhary S & Dhatarwal P, J Mol Liq, 252 (2018) 339.

13   Choudhary S, Dhatarwal P & Sengwa R J, *J Mol Liq*, 231 (2017) 491.

14   Sengwa R J, Dhatarwal P & Choudhary S, J Mol Liq 271 (2018) 128.

15   Iglesias T P & Reis J C R, *J Mol Liq*, 344 (2021) 117764.

16   Hevia F, Alonso V, González J A, Sanz L F, Fuente I G de la & Cobos J C, *J Mol Liq*, 322 (2021) 114988.

17   Gilani A G & Dafrazi A A, *J Chem Eng Data*, 65 (2020) 1886.

18   Jadżyn J & Świergiel J, *Ind Eng Chem Res*, 51 (2012) 807.

19   Chęcińska-Majak D, Bald A & Sengwa R J, *J Mol Liq*, 179 (2013) 72.

20   Jansson H, Bergman R & Swenson J, *J Mol Struct*, 972 (2010) 92.

21   Reis J C R, Iglesias T P, Douhéret G & Davis M I, *Phys Chem Chem Phys*, 11 (2009). 3977.

22   Sudo S, Shimomura M, Shinyashiki N & Yagihara S, *J Non-Cryst Solids*, 307–310, (2002) 356.

23   Choudhary S & Sengwa R J, *J Mol Liq*, 175 (2012) 33.

24   Huaxu L, Fuqiang W, Dong L, Jie Z & Jianyu T, *Int J Heat Mass Transf*, 128 (2019) 668.

25   Ibrahim P S S, Vinayagam S C, Murugan J S & Jeyakumar J E, *J Mol Liq*, 304 (2020) 112752.

26   Żyła G & Fal J, *Thermochim Acta*, 650 (2017) 106.

27   Gangwar J, Srivastava A K, Tripathi S K, Wan M & Yadav R R, *Appl Phys Lett*, 105 (2014) 063108.

28   Coelho M F, Rivas M A, Nogueira E M & Iglesias T P, *J Chem Thermodyn*, 158 (2021) 106423.

29   Akilu S, Baheta A T, Said M A M, Minea A A & Sharma K V, *Sol Energy Mater Sol Cells*, 179 (2018) 118.

30   Sengwa R J, Saraswat M & Dhatarwal P, *J Mol Liq*, 355 (2022) 118925.

31   Rosa D D, Wanic M, Fal J, Żyła G, Mercatelli L & Sani E, *Powder Technol*, 356 (2019) 508.

32   Rashin M N & Hemalatha J, *J Mol Liq*, 197 (2014) 257.

33   Yue H, Zhao Y, Ma X & Gong J, *Chem Soc Rev*, 41 (2012). 4218.

34   García J I, García-Marín H & Pires E, Green Chem, 16 (2014) 1007.

35   Sengwa R J, Sankhla S & Shinyashiki N, *Phys Chem Liq*, 48 (2010) 29.

36   Zhang T, Liu C, Gu Y & Jérôme F, *Green Chem*, 23 (2021) 7865.

37   Sengwa R J, Kaur K & Chaudhary R, *Polym Int*, 49 (2000) 599.

38   Sengwa R J, *Indian J Pure Appl Phys*, 41 (2003) 295.

39   Quispe C A G, Coronado C J R & Carvalho J A, *Renew Sust Energ Rev*, 27 (2013) 475.

40   Sengwa R J, Khatri V, Choudhary S & Sankhla S, *J Mol Liq*, 154 (2010) 117.
41   Jadżyn J & Świergiel J, *J Mol Liq*, 293 (2019) 111472.
42   Choudhary S & Sengwa R J, *J Mol Liq*, 167 (2012) 99.
43   Saraswat M & Sengwa R J, *J Mol Liq*, 368 (2022) 120671.
44   Murshed S M S & Estellé P, *Renew Sustain Energy Rev*, 76 (2017) 1134.
45   Sengwa R J & Saraswat M, *Particuology*, 76 (2023) 46.
46   Prajapati A N, Patel S P & Rana V A, *J Mol Liq*, 354 (2022) 118832.
47   Gilani A G & Mirkhalili A, *J Chem Eng Data*, 66 (2021) 3934.
48   Hevia F, Cobos A, González JA, Fuente I G de la & Sanz L F, J Mol Liq, 271 (2018) 704.
49   Sengwa R J, Chaudhary R & Mehrotra S C, *Mol Phys*, 99 (2001) 1805.
50   Pandey J D, Shukla A K, Singh N & Sanguri V, *J Mol Liq*, 315 (2020) 113585.
51   Makavana M & Sharma S, *J Mol Liq*, 222 (2016) 535.
52   Hussain S G M, Kumar R & Kannappan V, *J Mol Struct*, 1247 (2022) 131283.
53   Chaudhary N & Nain A K, *J Mol Liq*, 340 (2021) 116866.
54   Nithiyanantham S & Palaniappan L, *J Mol Liq*, 221 (2016) 401.
55   Belhadj D, Negadi A, Venkatesu P, Bahadur I & Negadi L, *J Mol Liq*, 330 (2021) 115436.
56   Saini A, Prabhune A, Mishra A P & Dey R, *J Mol Liq*, 323 (2021) 114593.
57   Kremer F & Schönhals A, Broadband Dielectric Spectroscopy, Springer-Verlag, Berlin, (2003).
58   Sengwa R J, Choudhary S & Dhatarwal P, *J Mol Liq*, 220 (2016) 1042.
59   Świergiel J, Bouteiller L & Jadżyn J, *Ind Eng Chem Res*, 52 (2013) 11974.
60   Jadżyn J & Świergiel J, *J Phys Chem B*, 115 (2011) 6623.
61   Ishai P B, Talary M S, Caduff A, Levy E & Feldman Y, *Meas Sci Technol*, 24, (2013) 102001.
62   Arrese-Igor S, Alegría A & Colmenero J, *J Mol Liq*, 318 (2020) 114215.
63   Benito J, Guerrero H, Artigas H, López M C & Lafuente C, *J Chem Thermodyn*, 86 (2015) 162.
64   Sengwa R J, Sankhla S & Choudhary S, *Colloid Polym Sci*, 287 (2009) 1013.
65   Świergiel J, Bouteiller L & Jadżyn J, *Soft Matter*, 10 (2014) 8457.
66   Hevia F, Alonso V, Cobos A, González J A, Sanz L F & Fuente I G de la, *J Chem Thermodyn*, 168 (2022) 106737.
67   Kumar M, Khan M A, Yadav C P, Pandey D K & Singh D, *J Chem Thermodyn*, 161 (2021) 106557.
68   Ayachit N H, Vasan S T, Sannaningannavar F M & Deshpande D K, *J Mol Liq*, 133 (2007) 134.
69   Reis J C R, Lampreia I, Santos A F S, Moita M L, Douhéret G, *Chem Phys Chem*, 11 (2010) 3722.
70   Pimentel G C, McClellan A L, The Hydrogen Bond, Freeman W H & Co, San Francisco, (1960).
71   Li H, Wang L, He Y, Hu Y, Zhu J & Jiang B, *Appl Therm Eng*, 88 (2015) 363.
72   Yan S R, Kalbasi R, Nguyen Q & Karimipour A, *J Mol Liq*, 308 (2020) 113058.
73   Reis J C R, Santos Â F S & Lampreia I M S, *Chem Phys Chem*, 11 (2010) 508.
74   Parmar D, Botchway C H, Dzade N Y, Kumari K, Maken S, Rani M & Kumar N, *J Mol Liq*, 347 (2022) 118279.
75   Douhéret G, Davis M I, Reis J C R & Blandamer M J, *Chem Phys Chem*, 2 (2001) 148.
76   Anu K & Hemalatha J, *J Mol Liq*, 256 (2018) 213.
77   Jacobson B, *J Chem Phys*, 20 (1952) 927.
78   Santhi N, Sabarathinam P, Alamelumangai G, Madhumitha J & Emayavaramban M, *Int Lett Chem Phys Astron*, 5 (2012) 1
79   Mukherjee S, Jana S, Mishra P C, Chaudhuri P & Chakrabarty S, *Int J Therm Sci*, 159 (2021) 106581.
80   Bridgman P W, *Proc Am Acad Arts Sci*, 59 (1923) 141.
81   Sakiadis B C & Coates J, Studies of thermal conductivity of liquids. Part I, *A I Ch E J*, 1 (1955) 275.
82   Bird R B, Stewart W E & Lightfoot E N, Transport Phenomena, 2nd Edn, John Wiley & Sons, New York, (2002).
83   Rao M R, *J Chem Phys*, 9 (1941) 682.
84   Wada Y, *J Phys Soc Jpn*, 4 (1949) 280.
85   Chithralekha N, Panneerselvam A, *Vacuum*, 168 (2019) 108835.
86   Kincaid J F, Eyring H, *J Chem Phys*, 6 (1938) 620.
87   Iglesias T P, Reis J C R & Fariña-Busto L, *J Chem Thermodyn*, 40 (2008) 1475.
88   Dubey G P & Dhingra L, *J Chem Thermodyn*, 149 (2020) 106161.
89   Meng X, Li X, Shi H, Wu J & Wu Z, *J Mol Liq*, 219 (2016) 677.
90   Tong A, Tang X, Zhang F & Wang B, *Spectrochim Acta A*, 234 (2020) 118259.
91   Li Q, Sha F, Zhao G, Yang M, Zhao L, Zhang Q & Zhang J, *J Chem Eng Data*, 61 (2016) 1718.
92   Arivazhagan G, Shanmugam R & Thenappan T, *J Mol Struct*, 990 (2011) 276.
93   Arivazhagan G & Thenappan T, *Phys Chem Liq*, 49 (2011) 275.
94   Li L, Zhang J, Li Q, Guo B, Zhao T & Sha F, *Thermochim Acta*, 590 (2014) 91.
95   Kuball H G, Höfer T & Kiesewalter S, Chiroptical spectroscopy, general theory, In Encyclopedia of Spectroscopy and Spectrometry (3rd Edn), Edited by Lindon J, Tranter G E & Koppenaal D, Elsevier Ltd, (2017) 217.
96   Saraswat M & Sengwa R J, *Phys E Low-dimen Syst Nanostruct*, 150 (2023) 115700.